Discrete element modelling of the steel/concrete bond with strong confinement.

ANDREA INVERNIZZI

N^ 725 508

Thesis

Presented in partial fulfilment to the requirements for the degree of
"Master of Science in Civil Engineering"

Polytechnic University of Milan - Lecco

October 2010

Project Advisor:

Francesco Calvetti **Polytechnic University of Milan**

Philippe Marin **Université Joseph Fourier**

Sylvain Gavoille **Université Joseph Fourier**

Acknowledgements

To my parents, Marta Donati & Salvatore Di Filippo, I gratefully dedicate this thesis. Thank you for always supporting me. I think it was worth it.

I wish to extend my warmest thanks to my colleagues Francesco Tagliaferri, Alessandro Tengattini and Silvio Verga , for whom I have great regard.

I would like to thank Sylvain Gavoille, Francesco Calvetti, Philippe Marin, Christian Geindreau, Cino Viggiani, Yann Malècot and Laurent Daudville for their support of this work.

Last but not least, I also wish to thank Ivan Donati for all his advise.

TABLE OF CONTENTS

PAGE:

1.Introduction ….....1

2. State of arts ….....3

2.1 Overview on concrete: material characteristics and used test.

2.2 Experimental results

2.3 Discrete Element Method

3.Pull-out test ….....37

3.1 Introduction

3.2 Concrete parameters calibration

3.3 Steel concrete interface parameters

4.Conclusion ….....46

List of figures **PAGE**

Figure 1: possible failure in the pull out test	4
Figure 2: Local Bond-Slip law [Gambarova 1989]	5
Figure 3,4 and 5 : behaviour of the materials at the interface	6
Figure 6 : specimen used.Bonded length L = 3Db	8
Figure 7: sketch of the specimen	17
Figure 8: interaction between two spheres	22
Figure 9: Geometrical characteristics	23
Figure 10: stiffnesses representation	23
Figure 11: steel representation with DEM	25
Figure 12: definition of the initial distance	26
Figure 13 : Sketch of Experimental specimen [Malvar , 1992] and specimens used for numerical computation	31
Figure 14: specimens representation	35
Figure 15 : link between concrete spheres	42
Figure 16: (a) real bar. (b) current method (c) hyp 1(D) hyp 2	45

List of graphs **PAGE**

graph 1: test results for δ_n = 0,1 mm,Phase C, Series 2.	8
Graph 2 : Bond and confinement curves obtained from Phase C test (average curves, Series 1 and 2)	9
Graph 3 : Typical diagram resulting from the tests with large diameter	10
Graph 4: Response curves for small diameter bars (a,b) and large diameter bars (c,d)	11
Graph 5: Test at constant confinement	12
Graph 6 : Test at constant confinement: linear regression of peak values of the bond stress-slip curves	12
Graph 7: Pull out test with transverse pressure	14
Graph 8 : Influence of transverse pressure	14
Graph 9: Analytical stress/slip curve	15
Graph 10 : maximum bond stress resistance	17
Graph 11: Ultimate frictional bond resistance	17
Graph 12: Series 1 Test P0 & P1	20
Graph 13: Series 2 Test 1-5	20
Graph 14: Series 3 test 6-10	20
Graph 15: Interaction laws	24

Graph 16 : Interaction law for steel	25
Graph 17:steel concrete interaction law. Normal force (a), tangential force (b)	26
Graph 18: experimental result L-3SR	28
Graph 19: experimental result L-3SR	28
Graph 20: compression test 30RA7	29
Graph 21 :Young's Modulus R30 A7	30
Graph 22: Poisson's ratio R30 A7	30
Graph 23 : Experimental and Numerical results	30
Graph 24: Study of velocity, high values	32
Graph 25: Study of velocity,low value	32
Graph 26: velocity influence in traction test	33
Graph 27 :Young' s modulus	33
Graph 28 : Poisson's Ratio	33
Graph 29: T influence	34
Graph 30: Co influence	34
Graph 31: Adou influence	34
Graph 32 :damping influence	35
Graph 33: mesh influence	36
Graph 34: TE	37
Graph 35: Tmax	37
Graph 36:Umax	37
Graph 37:Cn	38
Graph 38:Tn	38
Graph 39: Experimental and Numerical results.	38
Graph 40: BIMA[P0]. Zoom of the first slip part	39
Graph 41: concrete 1. BIMA with high value.	39
Graph 42: concrete 1. BIMA with high value. Zoom of the first slip part	40
Graph 43 : experimental and numerical curve .	41
Graph 44: Test 1 numerical and experimental curve	42
Graph 45: Test 1 numerical and experimental curve. Zoom of the first part	42
Graph 46 : Interaction law	42
Graph 47: influence of the concrete law	43

Graph 48: ADOU67.TN sensibility	44
Graph 49: ADOU200 .TN sensibility	44
Graph 50: modification proposed for the steel/concrete law	44

Abstract

The protection of structures such as nuclear power stations against external attacks like impacts of aircrafts can be improved. Better approaches must be developed to evaluate the ability of protective enclosures to withstand the design requirements under severe loading. In particular, we are interested in the safety of reinforced concrete structures . The sudden loss of bond can generate severe damage in the reinforced concrete . The present study focuses on steel/ concrete interface . For this study we use the discrete element modelling .It is well known that this method is reliable for the numerical representation of the concrete . Previous studies on steel/concrete interface has been done by [Rousseau, 2009] but it is observed that the law doesn't work with confinement. Based on the experimental results obtained by [Malvar 1992] and [Gambarova, 1989] the work presented here concerns the improvement of the modelling inside the DEM of the steel/concrete interface law. We present an approach to calibrate the steel/concrete interface with the Discrete Element Method. We remark also that to calibrate the bond/slip of the steel/concrete relationship when such radial pressure is applied we need to take into account the confinement law between the concrete particles.

Riassunto

La protezione di strutture soggette ad azioni dinamiche può essere migliorata. A tuttora i modelli che ci consentono di valutare la capacità resistente di una struttura soggetta a tali azioni potrebbero essere perfezionati. In questo studio l' interesse è legato a strutture in cemento armato ed in particolare verrà focalizzato sulla modellazione del legame tra acciaio calcestruzzo. Verrà utilizzato il modello a elementi discreti; dalla letteratura esistente [Rousseau, 2009] è noto che con tale modello è possibile rappresentare numericamente il comportamento in compressione ed in trazione del calcestruzzo e il comportamento dell' interfaccia acciaio calcestruzzo in una prova di pull-out.

Con le leggi esistenti [Rousseau, 2009] non è possibile rappresentare tramite DEM il legame acciaio calcestruzzo in presenza di confinamento laterale (attivo o passivo) . Basandoci su risultati sperimentali [Malvar, 1992] [Gambarova, 1989] si vogliono migliorare le leggi presenti per la modellazione numerica del legame di interfaccia acciaio calcestruzzo. Verrà inoltre presentato un approccio da utilizzare con il DEM per la calibrazione del legame acciaio calcestruzzo .

1. Introduction

This stage has been done in the L3S-R (Laboratory of Soils, Solid Structures and Risks). The L3S-R laboratory is specialised in geomechanics, civil engineering and associated risks as well as mechanical and multiphysics coupling in solid media. This is a mixed research team from the National Institute Polytechnic of Grenoble (INPG) , from Joseph Fourier University (UJF) and from the CNRS . In this laboratory the work focuses on the analysis and development of tools for optimization about the vulnerability of structures and systems, considering both the field of environmental and technological risks and the field of mechanical behaviour .

The protection of structures such as nuclear power stations against external attacks like impact of aircrafts can be improved. Methodologies must be developed to evaluate the ability of protective enclosures to withstand the design requirements .

For reinforced concrete structures, the sudden loss of connection between the steel reinforcement and concrete can generate severe damages to the structure. The objective of the present work is to improve the capability of the discrete element method to describe this kind of link. The choice of discrete element method is due to the fact that this method allows already to model appropriately the concrete failure for most of civil engineering structures [Schlangen 97,Mier 97].

Previous studies have already been conducted in this field by [Rousseau, 09] . The idea of the present study is, starting from such work, to extend its domain of validity .The aim is to overcome the observed lack of the bond law implementation, that , in the case of solicitations under strong confinement, loses his relevance. The application of such extension is, among the others, to gain a reliable discrete element modelling of the reinforced concrete to simulate impacts.

The outline of the present work is the following:

- Literature review of the references about steel/concrete interface tests under high confinement [Eligehausen '83, Gambarova '89, Malvar '92, Gambarova 96] to use as experimental data for our simulations.
- Analysis of the effects of the mesh construction parameters used in the EUROPLEXUS

simulations.

- Identification of material parameters used in the discrete element model to describe the concrete behaviour.
- Simulations of pull-out tests with confinement in the discrete elements model.
- Establishment of a new law steel-concrete interaction law to take into account the confinement.

2. State of art

2.1 Overview on the concrete , test used and bond mechanism

2.1.1 Introduction

The reinforced concrete is a widely used construction material in both civil and defence applications. It is constituted by a concrete matrix in which steel reinforcement bars have been incorporated to strengthen the concrete to tension states. The low cost, and high malleability of concrete, often makes it the best material for construction. Considering the works [Schlangen 97, Mier 97] we can conclude that, to study the macroscopic behaviour of concrete, an insight into microscopic process can be useful. Concrete is an heterogeneous material but it can be considered as homogeneous and continuous at the macroscopic scale .

2.1.2 Characterization of the concrete

The two main tests to identify the principal characteristics of concrete are :

- Compression test: performed on a 16*28 cm cylinder specimen, made of 28 days aged concrete, it consists of applying a compression force in the axial direction without applying any confinement .
- Tension test: performed on cylinder specimen,made of 28 days aged concrete, it consists of applying a traction axial force without applying any confinement .

They let us have an insight into the main elastic and plastic properties of concrete: Young's modulus E, Poisson's ratio ν ,maximum strength in traction f_t and in compression f_c .

2.1.3 Characterization of the steel concrete interface

When dealing with the steel/concrete interface, the common tests to study are:

- pull-out or push-in test
- beam test.

The two tests above mentioned will be briefly present leading to choice of the Pull-out test for the present work.

- **Pull out test**

In the pull out test , a bar with or without lugs is embedded in the middle of a concrete specimen (cylindrical or prismatic ,reinforced or not) and a load is applied (monotonic or cyclic) on the bar until the system brakes. The failure (figure 1) can occur for :

- "splitting, transverse & conic cracks" (macro-crack of the concrete)
- "pull out failure" (total extraction of the bar)
- yelding of the bar

This test consists of measuring the force in function of the slip applied at the end bar to deduce the behaviour at the steel/concrete interface.

The influence of the radial pressure applied on the concrete surface can be studied in this test (confining pull-out test)

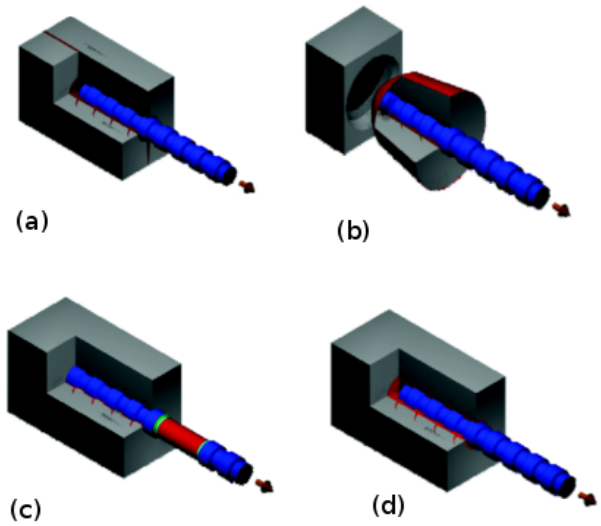

Figure 3: possible failure in the pull out test.
(a) longitudinal crack (b) conic cracks(c) plasticization of the bar (d) pull out failure [Dominiguez 2005]

- **The beam test**

Another popular test to study the steel concrete interface is the beam test.

The specimen used for this test consists in two symmetrical concrete parts joined together at the top by an hinge and at bottom by steel bars.

The specimen is supported at its two ends ; a vertical force is applied in the middle of the upper part. Measuring the displacement of the steel bar , knowing the applied force and the specimen geometry is possible to deduce the bond stress -slip path.

2.1.4 Bond mechanism

The interaction between the concrete and steel bar subject to a pull out force is characterized by four different stages [Gambarova,1989]:

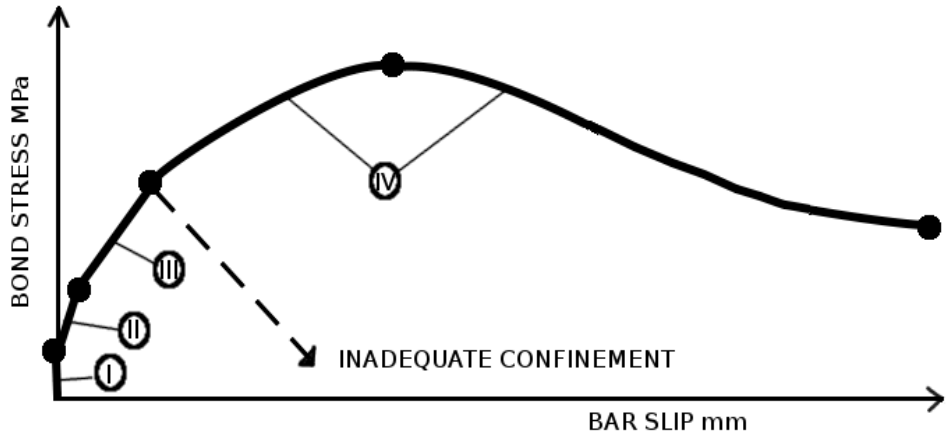

Figure 4: Local Bond-Slip law [Gambarova 1989]

At the point of view of the microscopic level is possible to note the following stages:

- stage 1: for small values of bond stress $\tau \leq (0{,}5\, to\, 0{,}8) f_{ct}$ no bar slip occurs. In this stage there is a perfect adherence between steel and concrete .
- stage 2: for larger values of bond stress $\tau = (0{,}7\, to\, 1.5) f_{ct}$ the lugs of the bar induce large bearing stresses in the concrete. The chemical adhesion breaks down and transverse microcracks, originate at the tip of the lugs, start to appear . The microcracks allows the bar to slip (figure 3).
- stage 3: for still larger values of bond stress $\tau = (1\, to\, 3) f_{ct}$ the first longitudinal cracks appears . Due to the build-up of the wedging action exerted by the bars and to the propagation of splitting cracks , all possible contribution to confinement are mobilized . The confinement efficiency depends on the concrete cover and bar spacing, on transverse reinforcement [Eligehausen, 1983] and on transverse pressure [Malvar , 1992] ,[Gambarova 1996] (figure 4)
- Stage 4: defined for bond stress values as large as $(1/3\, to\, 1/2) f'_c$. When the longitudinal crack reaches the outer borders of the concrete specimen the bond stress fails abruptly if no transverse reinforcement is provided. On the other hand , a sufficient amount of confinement action (passive or active) would assure bond efficiency in spite

of concrete splitting [Gambarova,1989]. Thus, with lateral confinement action, increasing the slip value the bond strength increases until a peak. In the post peak zone the stress decrease until the displacement of the bar is equal to the distance between the lugs. The last part of this phase is characterized by an asymptote . The bond resistance here is named frictional resistance (figure 5)

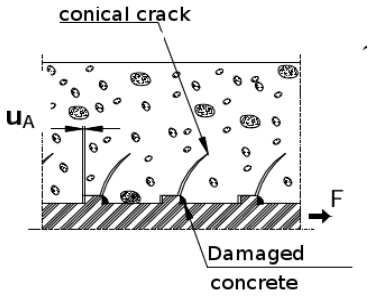

Figure 3: Second stage

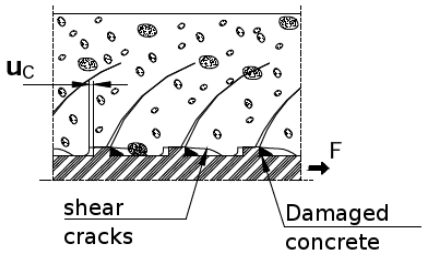

Figure 4: Third stage

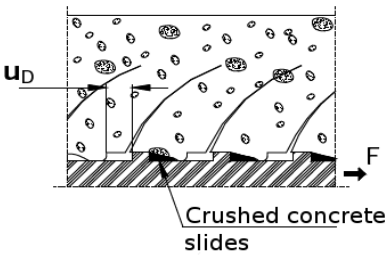

Figure 5: Fourth stage

2.2 Experimental results

2.2.1 Choice of the test

The pull-out test than the test beam seems achive this work for two main reasons:

- Experiments with a lateral pressure applied are done.
- The structural behaviour doesn't influence the results.

Therefore, we will be looking for the confining pull-out test results to calibrate the parameters in the DEM . Our work is mainly based on [Gambarova 1989], [Gambarova,1996] [Eligehausen, 1983] and [Malvar 1992].

- In the report [Gambarova ,1989] 19 pull-out tests are done to ascertain the basic properties of the bond resistance after concrete splitting. External confinement perpendicular to the longitudinal cracking plane allow the control of the longitudinal crack opening which is kept constant during each test. In particular are reported the results of pull-out test for specimens with a medium diameter bar $D_b = 18\text{mm}$
- In the report [Gambarova ,1996] 16 pull-out tests, with a small and a large diameter bars ($D_b = 14 - 24\,mm$), are carry out at a constant width of the splitting crack and variable pressure of confinement ; and 4 pull-out tests, with a medium diameter bar $D_b = 18\text{mm}$, are carry out at a constant confinement and variable width of the splitting crack.
- In the report [Eligehausen, 1983] 125 concrete specimens are tested .This study is the most complete work ever done about steel concrete-interface .It takes into account the variation of 7 physics variables that could influence the results.
- In the report [Malvar, 1992] 12 concrete specimens are tested. Among the others experiments that can be found in literature this is peculiar because :
  - Strong radial confinement pressure is applied (until 75 % f_c)
  - Two stages of loading are done to avoid the post peak discontinuity of the stress/slip curve caused by the appearance of the first longitudinal crack.

2.2.2 Overview of [Gambarova, 1989] : "Steel-to-concrete bond after concrete splitting: test results"

In the report of [Gambarova 1989] the results of 19 pullout test are discussed. Each specimen consists of two parts of concrete, which are in contact with the single reinforced bar in a limited zone (figure 6). Twelve specimen (Test A and C) are fitted up with round deformed bar having a crescent -shaped lugs (D_b = 18 mm) and seven (test B) are fitted up with a specially machined deformed bar having a rectangular cross section and straight lugs. Is interesting to note that only by testing precracked specimens the four basic parameters (crack opening, bar slip, bond stress and confinement) can be controlled separately, in order to investigate their interaction [Gambarova ,1997].

In [Gambarova 1989] are reported the test results of the test C whilst the details of the test A and B are reported in [Gambarova ,1982] and [Gambarova, 1983].

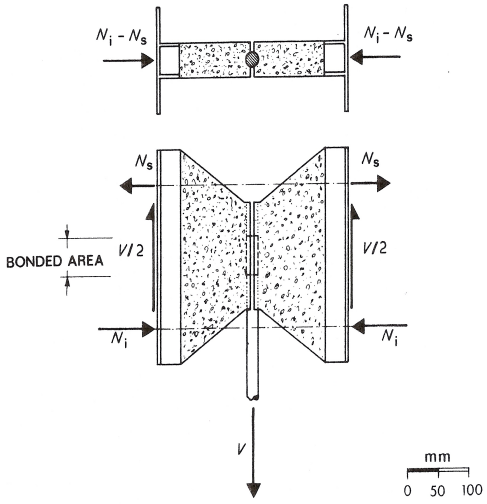

Figure 6 : specimen used.
Bonded length L = 3Db

In the test C a couple of experiments are done for each of the four different cracks opening (δ_n = 0.0, 0.1, 0.2, 0.3 mm). The opening of this crack is maintained at a prescribed width while tensile load is applied to one end of the reinforcing bar under displacement control. Applied load is reacted through shear on the surfaces of the concrete prism parallel to the crack plane. Slip is measured as the movement of the unloaded bar end with respect to the concrete prism . During each experiment are measured the stresses (bond and confinement) at the bar-to-concrete interface at increasing bar slip ($\delta_l \leq (0{,}2\, to\, 0{,}30)\, D_b$).

The characteristics of the materials are :

for the concrete the compressive strength is $f_c' = 40{,}2\, Mpa$ and a tensile strength is $f_{ct} = 4{,}5\, Mpa$ while for the reinforcements bars the yield strength is 430 Mpa. In (7) are shown the curve relating the pull out force V and the confinement force N to slip :

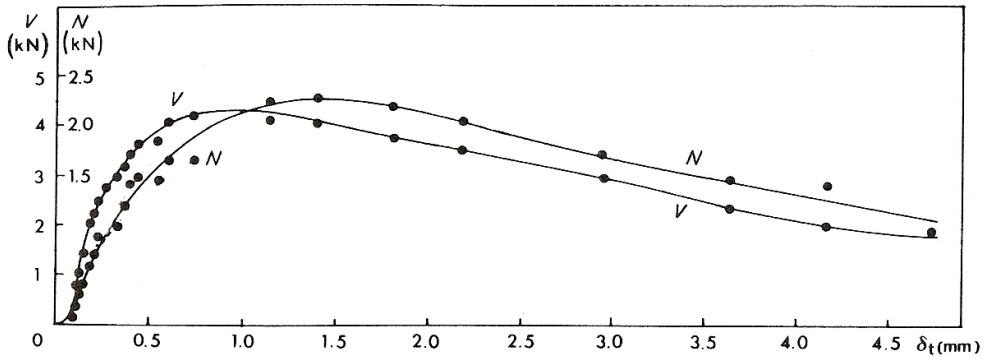

graph 1: test results for δ_n = 0,1 mm,Phase C, Series 2.

From these forces (pull out V and confinement N) is possible to evaluate the stresses :

$$\tau = \frac{T}{\pi d_b L} \qquad \sigma = \frac{2N}{\pi d_b L}$$

Where: τ is the bond stress, σ is the confinement stress, d_b and L are the diameter and the bonded length of the reinforced bar.

The graph 2 shows the bond stress versus slip and radial stress versus slip obtained in test C.

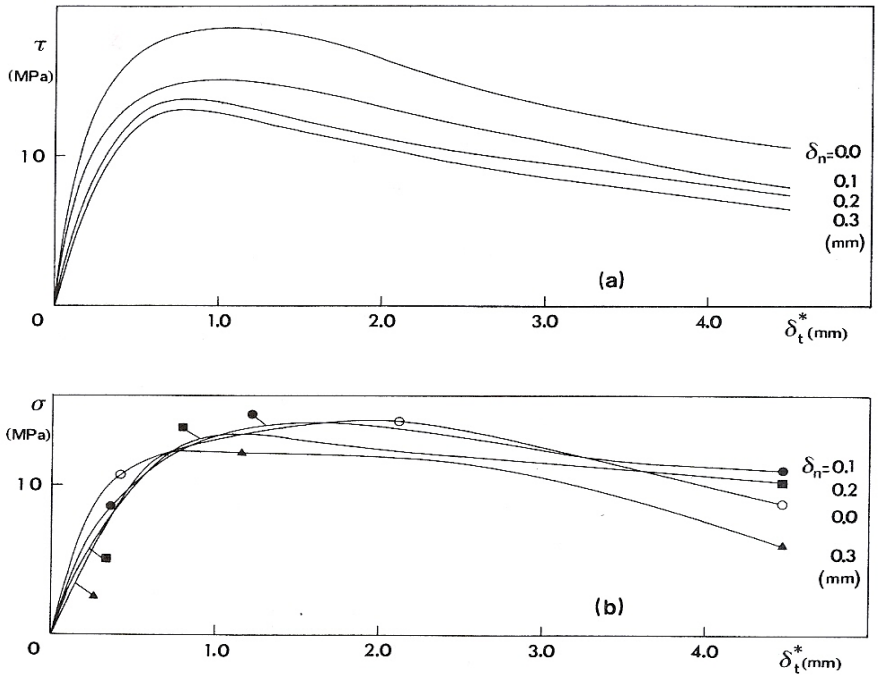

Graph 2 : Bond and confinement curves obtained from Phase C test
(average curves, Series 1 and 2)

Observations on the results:

- The bond strength decrease at increasing of the splitting crack opening.
- The peak value of the confinement stress is not strongly dependent of the splitting crack.

2.2.3 Overview of [Gambarova, 1996] "Bond and splitting in reinforced concrete: test results on bar pull Out":

In the report of [Gambarova, 1996] are presented the result regarding the behaviour of bond stress in lateral confinement pull out test. In this study 20 specimens were tested ,16 reinforced by a 24 –14 mm bar (test E and D at constant opening of the splitting crack) and 4 reinforced by an 18 -mm bar (test F at variable opening and at constant confinement crack)

The specimens have a parallelepiped shape and only five lugs of the bar are in contact with the concrete (figure 6) .

The concrete compressive strength f'_c is equal to 38-52 Mpa and a f_{ct} is equal to 3.1-3.8 Mpa. The steel yield strength is 432 Mpa. The tests are force-controlled up to the peak of the load slip response and displacement controlled after the peak.

The objective of this article is first of all perform a test to have a data base instrumental in the formulation of :local bond-slip and confinement-slip law at constant crack opening . A second objective of this study is to investigate if the static response (confinement, σ , and bond , τ , stress) depends on the kinematic path (nominal opening of the splitting crack δ_n and bar slip, δ_t), for the same final displacements. The third objective ,closely related to last one, is to check if bond strength (τ_{max}) depends on the confinement level (σ = constant).

Results of the tests:

- Constant width of the splitting crack opening . An example of test results are shown in (graph 3)

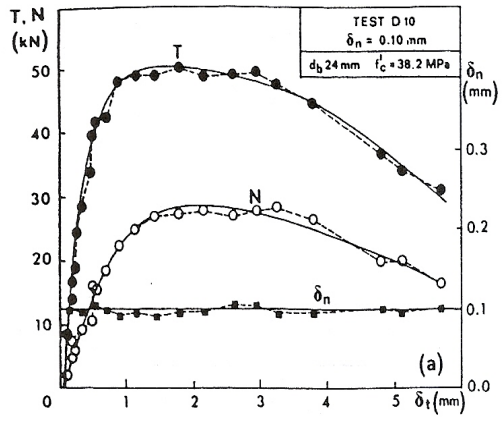

Graph 3 : Typical diagram resulting from the tests with large diameter bars. Test D10

where:

δ_n width of the performed splitting crack

δ_t total bar slip

Basing on the assumption that the applied forces are uniformly distributed along the bonded surface of the bar is possible to deduce the stresses τ and σ through the following self explanatory equations:

$$\tau = \frac{T}{\pi d_b L} \qquad \sigma = \frac{2N}{\pi d_b L}$$

Where: τ is the bond stress, σ is the confinement stress, d_b and L are the diameter and the bonded length of the reinforced bar.

In the following diagrams the stress -strain curves are represented. Each curve is the average of the curves related to two nominally identical specimens.

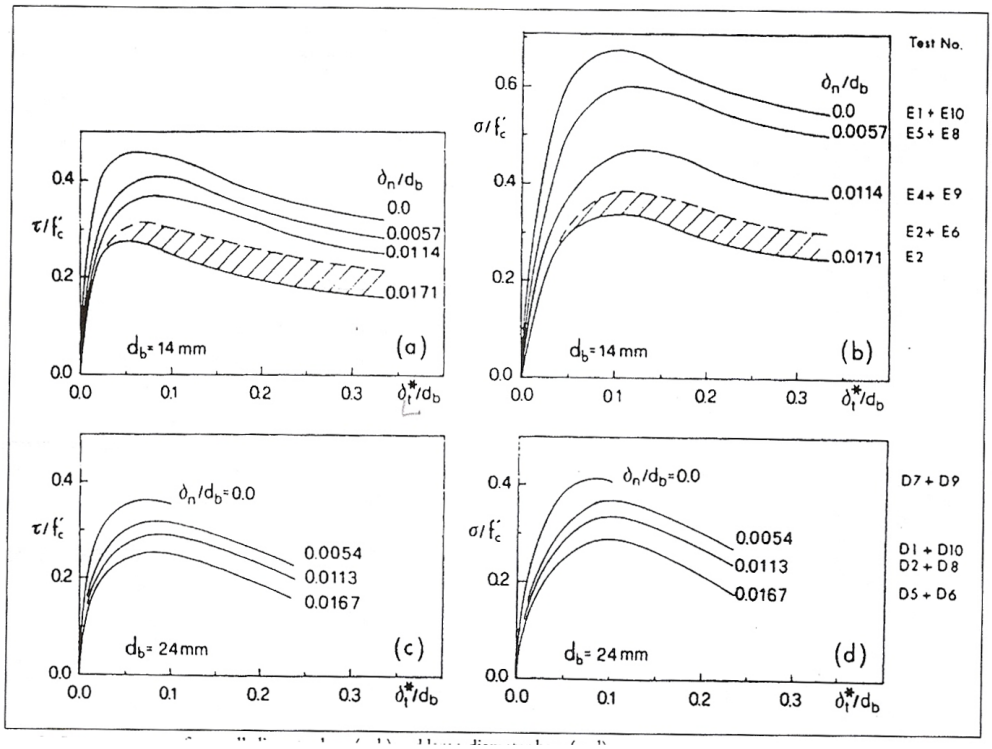

Graph 4: Response curves for small diameter bars (a,b) and large diameter bars (c,d)

- Constant confinement : for this study 4 specimens are tested in order to determine the bond behaviour (table 1).

  In the test F4 the kinematic path is different, since attention is focused on the confinement degree,which is kept as close as possible to 0,205 σ / f'_c .

MAIN DATA OF CONSTANT CONFINEMENT TESTS (in =initial, av=average,sd = standard deviation)					
TEST	$(\sigma / f'_c)_{initial}$	$(\sigma / f'_c)_{avara}$	(τ_{max} / f'_c)	$(\sigma / f'_c)_{sd}$	$f'c(MPa)$
F1	0,000	0,091	0,168	0,21	38,2
F2	0,144	0,115	0,200	0,22	38,2
F3	0,205	0,200	0,332	0,19	41,6
F4	0,205	0,216	0,300	0,08	41,6

Table 1

In the (graphs 5,6)the stress-opening curves resulting from Test F1-F3 are plotted:

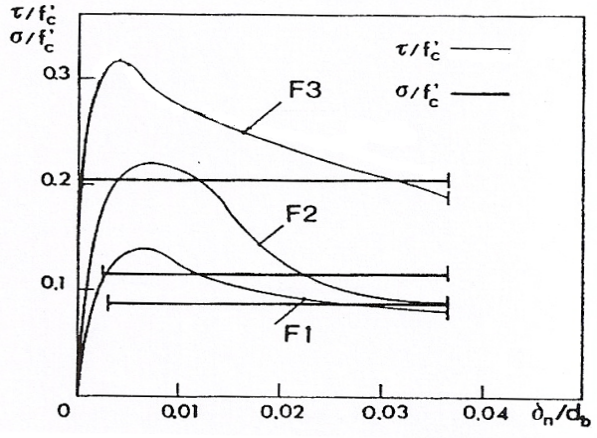

Graph 5: Test at constant confinement

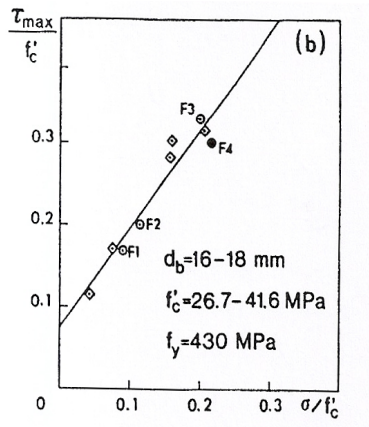

Graph 6 : Test at constant confinement: linear regression of peak values of the bond stress-slip curves

Where: δ_n width of the performed splitting crack, τ is the bond stress, σ is the confinement stress, d_b is the diameter of the reinforced bar and f'_c is the concrete cylindrical strength in compression.

Observations on the results:

- the bond stress-slip response of the bar is adversely affected by the opening of the splitting crack, more for large diameter than small-diameter bars.

- In the tests at constant confinement, bond strength (peak value of the sbond-slip response) is a linear function of the confinement stress.

- Bond path dependency: Bond static response is not markedly affected by the kinematic path on the condition that the confinement is quite large .

2.2.4 Overview of [Eligehausen, 1983] : "Local Bond Stress-Slip Relationships of deformed bars in Concrete"

Experimental results

In the report of [Eligehausen, 1983] the tests of 125 specimens consisting of one single bar casted in a well confined concrete block . The bar undergoes a monotonic or cycling loading . Only a short length (5 times the diameter d_b) of a deformed reinforcing bar is embedded in the confined concrete . The bar is surrounded by steel reinforcement . The concrete have a maximum resistance f_c equal to 30 MPa. The steel has a yield strength equal to 530 MPa, the maximum strength reached in the tests is well below this value. The specimen is installed in a hydraulic testing machine used under displacement control.
The influence of the following parameters on the bond via stress/slip relationship has been studied:

- Test in tension or compression loading: the bond stress-slip relationship of pushed bars is almost identical to that of pulled bars for slip values < 0.1 mm and slightly lower for larger slip values. Evaluation of Poisson effect on the bond was not studied in these experiments.
- Confining Reinforcement: there is a huge difference for test with or without confining reinforcement . Increasing the diameter of the vertical bars increases the stress bond . The test shows that there is an upper limit for an effective restraining reinforcement beyond which the bond behaviour cannot be improved. Specimen without reinforcement failed by splitting of the concrete at a rather small bond stress.
- Bar diameter: the maximum bond stress decreased slightly with increasing the bar diameter. The frictional bond resistance was not influenced much. Eligehausen note also the increasing of the slope of the ascending part of the stress-slip graph.
- Concrete strength: by increasing the strength of the concrete, it is noted that the maximum bond resistance is reached at smaller slip values. The increase in bond resistance is about 35 %, which is almost equal to the increase in tensile strength of the high strength concrete compared to the normal one.
- Bar spacing: the bond behaviour improves by increasing the bar spacing, increasing the

bar spacing from s= 1d_b to s=4d_b bond resistance increased by about 20%; further increase have no effect.

- Transverse pressure: the pressure is ranging from p= 0 MPa to p = 13.2 MPa. Such pressure is applied only on the faces perpendicular to the direction of the principal bar. The idea is to reproduce the beam column joint . The applied maximum pressure is equal about 45 % of the compressive strength.

  Bond stress diagrams were deduced taking applied forces at given slip values, (graphs 7-8) .

- Rate of pull out velocity : bond resistance increasing by increasing the rate of pull out velocity.

- Influence of the history with cyclic loading: During cyclic loading, the degradation of the resistance and the stiffness of the interface depend primarily on the maximum displacement beforehand. Other parameters such as number of cycles and the difference between the peaks of alternate displacement are also significant. If the loading cycles are realized with displacement equal or less than 80% of the maximum shear stress reached under monotonic loading, the reduction of the resistance is moderate and does not really affect the behaviour of the bond at major shifting. N/mm^2

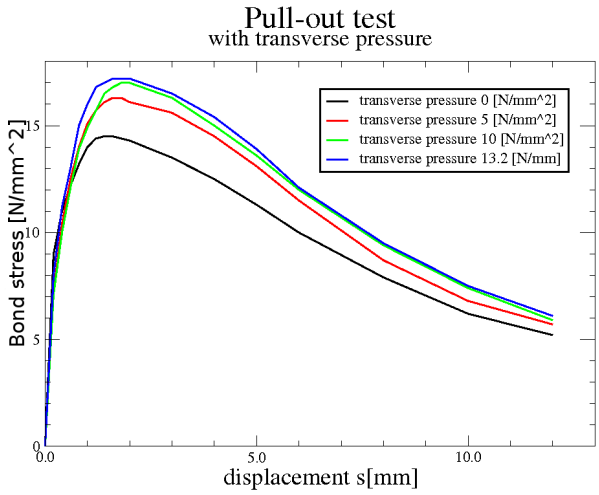

Graph 7: Pull out test with transverse pressure

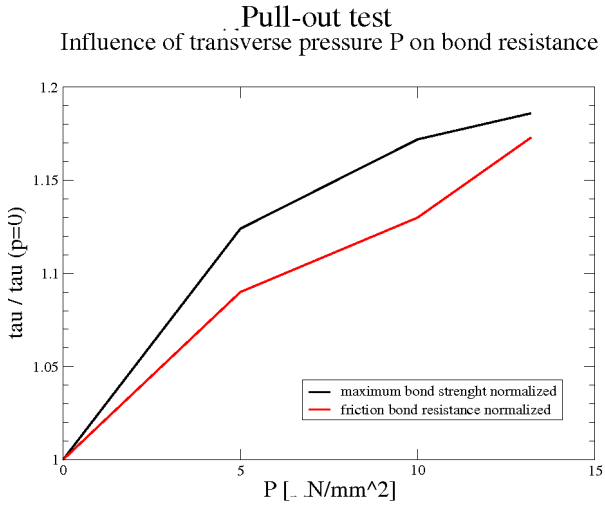

Graph 8 : Influence of transverse pressure

Analytical model for confined concrete

The bond stress-slip curve in (graph 9) is made of a non linear initial part (represented by the equation 1) :

$$\tau = \tau_{max}\left(\frac{s}{s1}\right)^{\alpha} \qquad s < s_1 \qquad (equation\ 1)$$

This part is followed by a plateau at $\tau = \tau_{max}$. For a slip range between $s_2 < s < s_3$, τ decreases linearly to the value of the ultimate frictional bond resistance . For $s > s_3$ the bond resistance τ keeps a constant value of τ_{frict} . The slip value s_3 is assumed to be equal to the clear distance between the lugs of the deformed bars.

Value find in [Eligehausen, 1983] for a non confinement pull out test (bar diameter 25 mm):

s_1 = 1.0 mm

s_2 = 3.0 mm

s_3 = 10.5 mm

τ_{max} = 13.5 MPa

τ_{frict} = 5.0 MPa

α = 0.40

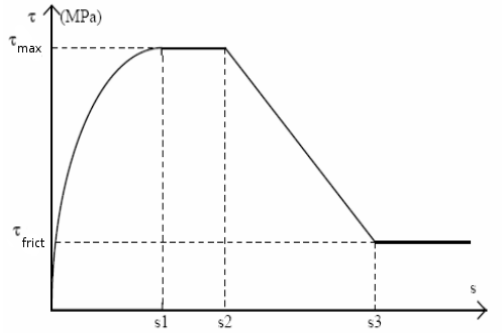

Graph 9: Analytical stress/slip curve

The influence of external transverse pressure can be taken into account by increasing τ_{max} and τ_{frict} according with (Graph 9) . It is worth to note (Graph 8) that the bond strength is more affected by the pressure level for low and medium confinement levels than at high level .

If the bar diameter changes also the bond stress will change, in particular in [Eligehausen, 1983] is proposed the increment of τ_{max} by 10% if bars with diameter d_b = 19 mm are used instead of 25 mm and the decrement τ_{max} by 10% if bars with diameter d_b = 32mm are used .

Also the geometry of the outer surface of the bar is important. The shape and the position of the lugs plays a role in the crack pattern; their influence in the bond stress – slip pattern is shown both in [Eligehausen, 1983] and in [Malvar 1992].

Assessment of the transverse pressure influence

In (graph 7- 8) we can see that arise of the pressure increases the maximum bond resistance.

It is also interesting to note that (graph 8), the ratio $\frac{\tau_{max}(P)}{\tau_{max}(P=0)}$ decreases when transverse pressure raises. For the slope $\frac{\tau_{frict}(P)}{\tau_{frict}(P=0)}$ we find slightly different values .This can probably be attributed to the scatter of the test result.

In graph 10 the experimental results of [Eligehausen, 1983] are compared with the results of other investigations. We can note that the increase of frictional bond resistance caused by transverse pressure, in different experimental investigations, have a remarkable scatter. For a transverse pressure equal to 10 Mpa the bond strength ranges moreless from 2.5 Mpa to 8.5 Mpa.

In the test of [Untrauer/Henry 1965], specimens fail by pulling out of the bars only when there is sufficient normal pressure. If failure would be caused in all test by pull-out , the influence of transverse pressure on τ_{max} would have been much smaller than shown in (graph 10, line 4).

In the test of [Viwathenatepe 1979] and [Cowell 1982] a transverse pressure is induced by a bending moment . The bar is also yielding in compression . Therefore, the results are influenced by the internal pressure due to the expansion of the bar. The increase of τ_{max} observed by [Doerr 1978] at 15 Mpa seems unrealistically high in comparison to the other two values of the same test and in contradiction with the general trend found in the other investigation.

Additional tests are necessary to study the influence of external pressure and internal pressure due to the Poisson's ratio effect which should be investigated separately.

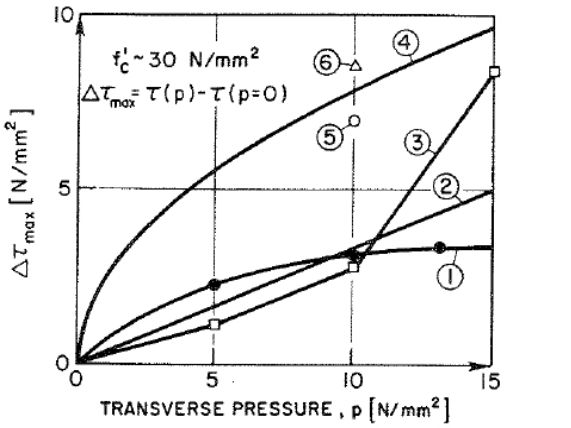

Graph 10 : maximum bond stress resistance

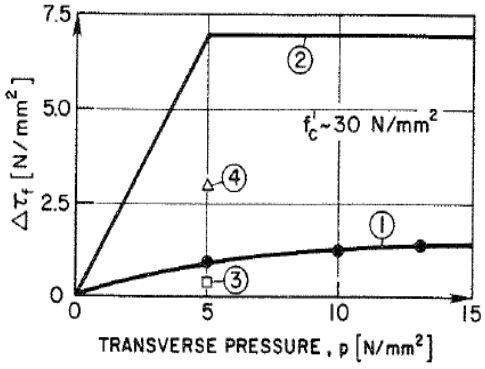

Graph 11: Ultimate frictional bond resistance

2.2.5 Overview of [Malvar ,1992] : " Bond of Reinforcement Under Controlled Confinement "

Experimental setup

In this paper 12 specimens are tested in order to determine the local bond stress-slip features. The diameter of the steel bar is 19 mm and the concrete specimen has a diameter of 76.2 mm and a height of 101.6 mm (figure 7). These tests are studied both under the influence of radial confining stress around the concrete specimen and the radial deformation . Five lugs are in contacts with the concrete, while such a link is prevented in the rest of the sample by inserting two silicone rubber spacers around the bars allowing inclined radial cracks to form at each rib to propagate to the external concrete surface.

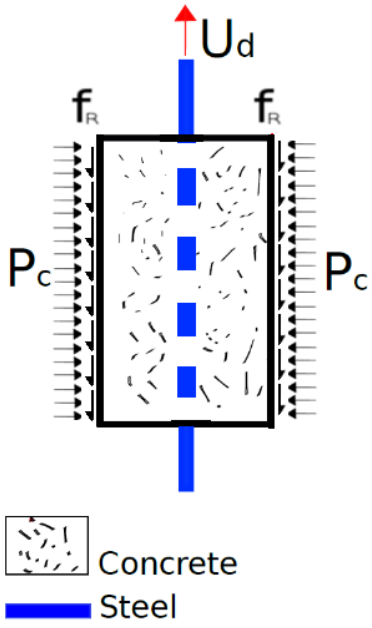

Figure 7: sketch of the specimen

The outer surface is surrounded by a threaded steel pipe that carries the load and hold concrete back thanks to the frictional resistance. The pipe is divided longitudinally in eight stripes . The equivalent confining pressure given by the strips , less than 0.87 Pa, has a negligible effect on the results.

Two LVDT are installed, one for measuring longitudinal displacement and another for the radial one. On one end of the specimen, the bar is threaded and bolted to the testing device cross -head. On the other end ,the inner of the split pipe is threaded and bolted to the piston.

2.3.2 Test series

The tests are divided in 3 series :

- series 1 : in these series two test are done, test P0 and P1. These are carried out to get reference values. Bars with inclined ribs that have a 68-deg angle with longitudinal axis are used
- series 2 : test 1- 5: Bars with inclined ribs that have a 68-deg angle with longitudinal axis are used
- series 3 : test 6- 10: Bars with inclined ribs that have a 90-deg angle with longitudinal axis are used

The material properties of the concrete specimens are reported in Table 2 :

	E [GPa]	**ν**	**Fc Mpa**	**Ft Mpa**	**ρ kg/m³**
Test P0 - P1	29	0.2	44.0	5.0	2192
Test 1- 5	28	0.2	40.0	4.9	2192
Test 6-10	27	0.2	38.4	4.7	2192

Table 2

Test P0 and P1 are monotonic load to failure under respectively 0 and 6.8 Mpa constant external radial pressure at the bar surface .

For the other two series **test 1-5** & **test 6-10** two stages of loading are applied. First stages are until the longitudinal crack forms, then unloaded. During this stage some confinement is provided by the concrete cylinder itself. During the second stage the load is monotonically applied until slip reached about 12 mm. In the following table are reported the values of the pressure for each test.

	Lateral Pressure P_c (Pre cracking phase) [MPa]	Lateral Pressure P_c (Post cracking phase) [MPa]
Test 1	3.45	3.45
Test 2	10.34	10.34
Test 3	17.24	17.24
Test 4	24.1	24.1
Test 5	31.03	31.03
Test 6	3.45	3.45
Test 7	fail	fail
Test 8	3.45	17.24
Test 9	3.45	24.1
Test 10	3.45	31.03

Table 3

The author remark that the total confinement before cracking is variable because it is a combination between concrete cylinder confinement and the externally applied one .

Due to this reason in this experiment two stages of loading have been done. In the second stage the concrete does not provide any confinement and the applied radial pressure transfers straightly to the bar surface.

2.3.3 Remarks on the results

- Test P0 & P1 : lateral confinement applied in test P1 changes a lot the response of the test. The bond resistance increase with the raise of lateral confinement (Graph 12)
- Influence of the rib spacing on the frictional resistance; the bond stress then decrease until the slip is approximately equal to the clear rib spacing (9.2 or 10.2 mm for tests 1-5 and 6 - 10, respectively).
- Bond stress is typically higher for the bars with normal ribs at an angle of 90 deg with the bar axis than for the 68° deg bars (Graph 13-14).
- In Test 5 and 10 (the two with higher confinements) the author note that the post peak decay fastly (Graph 13-14).

- In the post-cracking range,the effect of confinement on bond behaviour appeared less pronounced for higher confining stress. The author attributed this phenomena to the faster degradation produced by high confinement

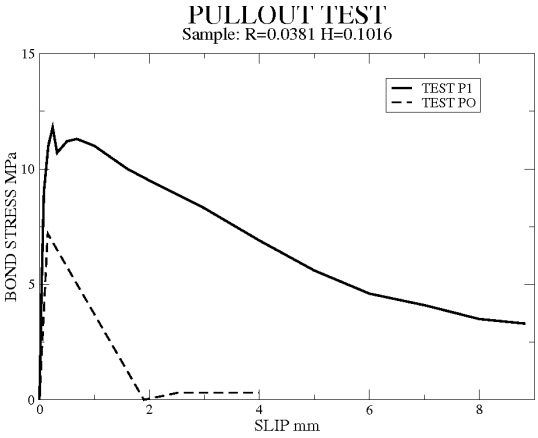

Graph 12: Series 1 Test P0 & P1

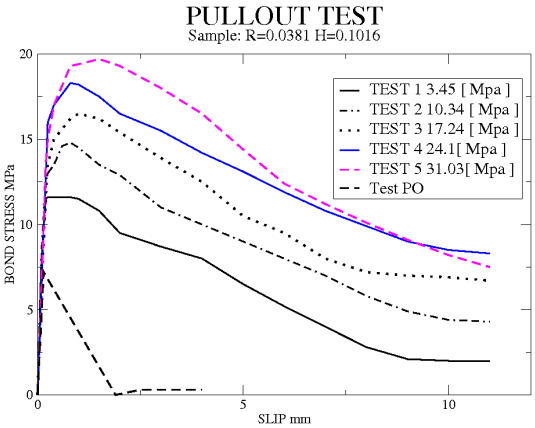

Graph 13: Series 2 Test 1-5

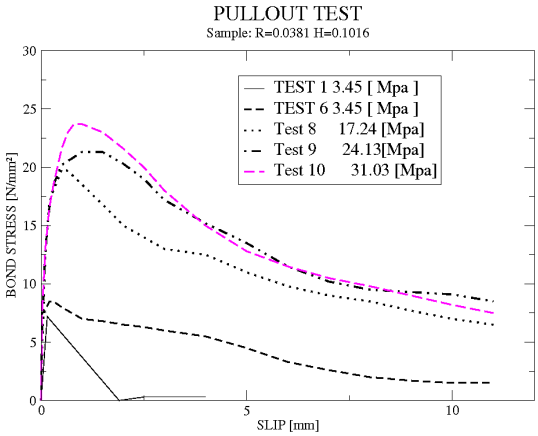

Graph 14: Series 3 test 6-10

2.3 Discrete Element Method

2.3.1 Introduction

The design of some civil engineering structures requires to take into account the solicitation of severe loadings linked to a natural or anthropogenic hazard such as a rock fall, aircraft or missile impact

This kind of loading can generate a huge damage in the concrete and the consequences can be disastrous. Therefore it is very important to model the structure behaviour in order to strengthen the building where it is necessary. Thus, reinforced concrete behaviour has to be modelled with accuracy. Damages like cracks and fragmentations remain uneasy to represent with continuous mechanics methods while the DEM is able to represent fractures in geomaterials like concrete .

The basic idea of the DEM is to reproduces the mechanics of contacts between distinct elements. Materials like rock, concrete and soil can be regarded as an assembly of such discrete grains, therefore the discrete element method have a huge potential in their modelling.

Using the discrete element method we want to identify the parameters that allows us to describe the behaviour of steel/concrete interface when a pressure is applied at the outer surface of the bar.

2.3.2 The discrete element method

Discrete Element method can be splitted up into two group: lattice model and distinct element model.

Lattice model

The link used by this model is a beam or a bar organized in a structural network.

A local behaviour is affected to each link and a rupture criterion allows to take away broken link of the model. In their model , [Prado, 2003] used a Euler-Bernoulli beam with elastic brittle constitutive behaviour.

[Cusatis, 2007] propose the “Confinement Shear Lattice model”. They only consider the biggest aggregate and connect their centroids with structural element. In the lattice model the calculation effort is relevant , especially to determine constitutive behaviour parameters.

Distinct Element model

In the early developments of this method for non-cohesive materials like sand [Cundall ,1979], particles interactions were described by normal repulsion and friction laws. Afterwards, the interaction law for cohesive materials have been refined [Hentz, 2003].

The shape of the particles are of a great importance in the evaluation of the contact surface. It is possible to use different types of shape e.g. circular shape, ellipsoids or polyhedrons.

With the circular shape the determination of contact is very fast, the polyhedron the determination of the contact requires a lot of time. To guarantee reasonable computational times, a model based on Distinct Elements Model [Cundall, 1979] with rigid sphere is chosen in the present work.

The basic idea of the method is that bodies interact (figure 8) with each other by means of some physical laws, which describe the interaction responses . Such as interaction influences each body and change their kinematical behaviour like position velocity or acceleration.

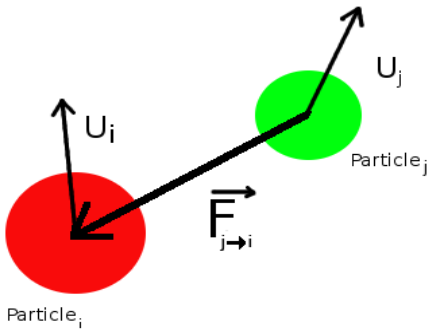

Figure 8: interaction between two spheres

The equation 1 allow us to determine the force $\underline{F_i^j}$ on the particle **"i"** due to the particle **"j".** The particles **"j"** are defined taking into account the interaction ratio.

$$\underline{F_i^j} = \boldsymbol{K}_r\left(\underline{\Delta_i^j}\right) + \boldsymbol{K}_m\left(\underline{\Delta\theta_i^j}\right) \qquad \textit{equation } 1$$

Where:

$\boldsymbol{K}_r$ is the stiffness matrix and can be different between:

- concrete
- steel
- steel/concrete interface

$\underline{\Delta_i^j}$ is the difference of displacement between particle **"i"** and **"j"** , the particle **"j"** are defined by the law with interaction radius

$\boldsymbol{K}_m$ is the stiffness matrix for the rotation

$\underline{\Delta\theta_i^j}$ is the difference of rotation

When the force is calculated it is possible to determine the acceleration, a_i of the particle **"i"** with the equation 2 :

$$\underline{a_i} = \frac{1}{m_i}\left(\Sigma_j \underline{F_j^i} + F_{ext}\right) \qquad equation\,2$$

where :

$\underline{F_j^i}$ is the interior force

F_{ext} is the exterior force

A newmark schema is used for the discretization of the time.

2.3.3 The discrete element model used for this work

The method presented in the following was designed by [Hentz, 2003] and [Rousseau, 2009]. The material is represented by a set of spheres , with different dimension and random distribution, that interact with each other trough a cohesive and a contact law. The law that govern the spheres movement changes with the material considered . Now we will explain how concrete , steel and steel/concrete interface are represented .

a) Concrete

Interaction between two spheres are defined by two stiffness: the normal one K_n and the tangential one K_s . They are linked with macroscopic parameters like the modulus of elasticity E and the Poisson's ratio υ . Relations, named "micro-macro", are defined in (equation 4) .

$$\begin{cases} E = \left(\dfrac{D_{eq}}{S_{init}} k_n \dfrac{(\beta + \gamma \dfrac{k_s}{k_n})}{(\alpha + \dfrac{k_s}{k_n})} \right) \\ \nu = \left(\dfrac{(\beta + \gamma \dfrac{k_s}{k_n})}{(\alpha + \dfrac{k_s}{k_n})} \right) \end{cases}$$

equation 3

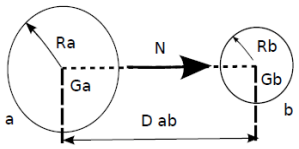

Figure 9: Geometrical characteristics

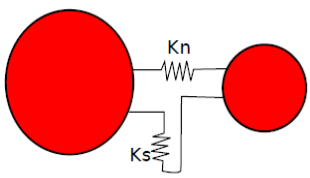

Figure 10: stiffnesses representation

In equation 3 D_{eq} is the initial distance between the particles , $S_{inter} = min\left(\pi R_a^2, \pi R_b^2\right)$ and α, β, γ are parameters related to the radius of interaction between particles [Rousseau, 2009] .

Then , after the definitions of the links between the particles, it is necessary to define when the links will be broken.

$$\begin{cases} f_1(F_n, Fs) = Fs - \tan(\Phi_i) F_n - S_{inte} C_o & plasticity\ criterion \\ f_2(F_n, Fs) = S_{inter} T - F_n & failure\ criterion \end{cases}$$

(equation 4)

$$\begin{cases} if\ f_2(F_n, Fs) \le 0 & cohesive - elastic\ link \\ if\ f_1(F_n, Fs) \ge 0 \wedge f_2(F_n, Fs) < 0 & F_s \tan(\Phi_i) F_n - S_{inter} C_o \\ if\ f_2(F_n, Fs) < 0 & rupture\ (F_s = F_n = 0) \end{cases}$$

(equation 5)

Where C_O is the cohesion factor, Φ_I the frictional angle , T the local tensile limit and F_n and F_s are the tangential and normal loads. We remark that a softening factor ς is introduced in the law to represent a tensile effort progressively going to zero. When the cohesive link is broken we have a new contact interaction between DE and the friction angle Φ_c .

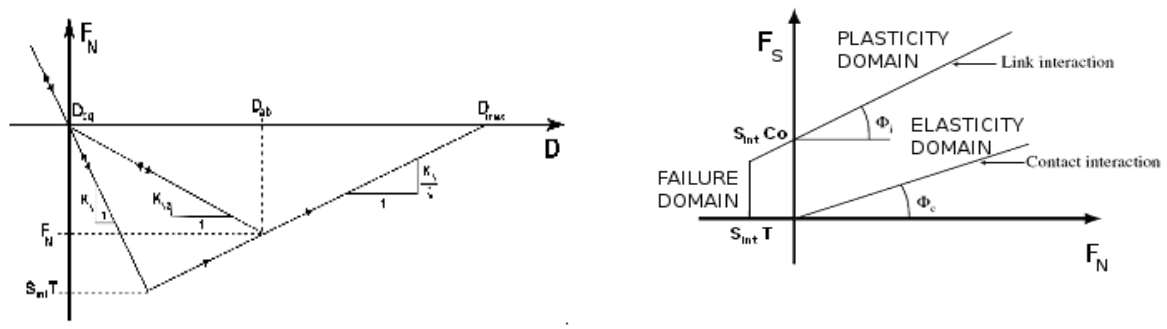

Graph 15: Interaction laws

b) Steel

The modelling of the steel bar is done with a group of aligned spheres with the same radius , illustration at (figure 11). The equations used for the stiffness between the DE spheres is defined in equation 6:

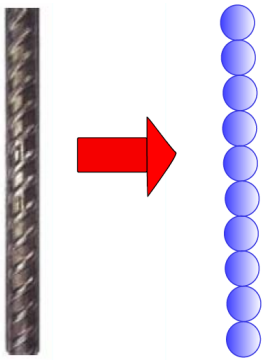

Figure 11: steel representation with DEM

$$\begin{cases} K_n = \dfrac{ES_{inter}}{D_{eq}} \\ K_s = \dfrac{ES_{inter}}{(D_{eq}\,2\,(1+\nu))} \end{cases}$$

equation 6

Where S_{inter} is the surface of interaction between the spheres and D_{eq} is their initial distance.

The elasto-plastic law that characterizes the steel is plotted in the graph 16 :

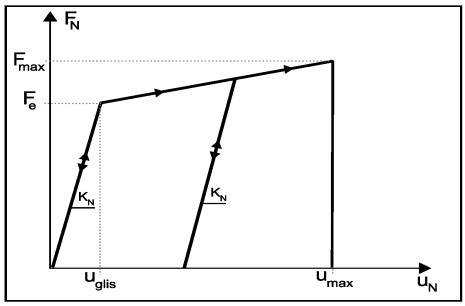

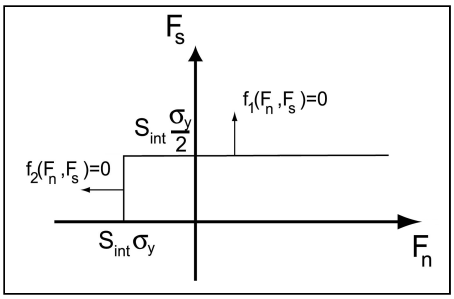

graph 16 : Interaction law for steel

The model described in the graphs represents :

-An elastic behaviour $F_e = S_{int.} f_e$ $F_N < F_e$ $(equation\ 7)$

-An hardening behaviour $F_{max} = S_{int.} f_{max}$ $F_e < F_N < F_{max}$ $(equation\ 8)$

c) Steel concrete interface

Considering the work of [Rousseau,2009] , we assume that the discrete element law between steel & concrete like in (graph 17) :

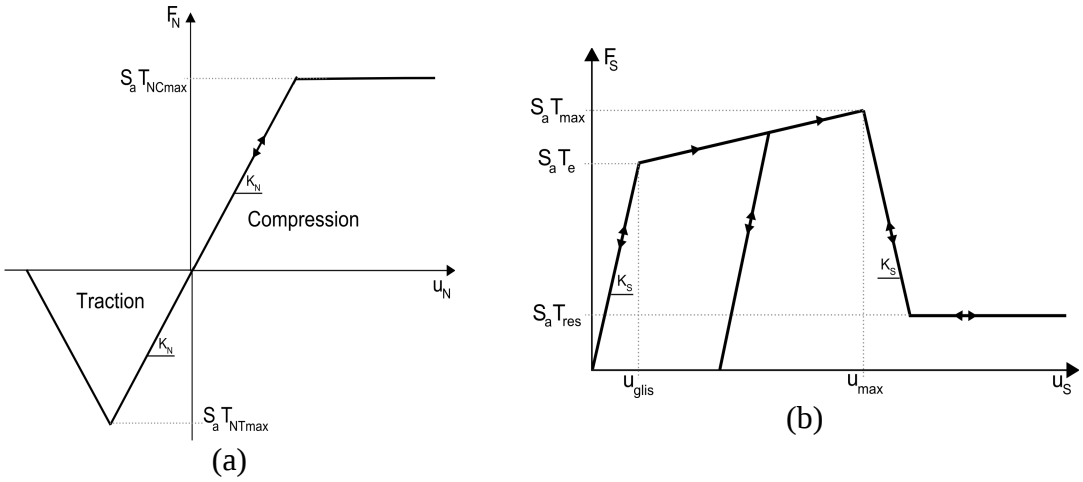

graph 17: steel concrete interaction law. Normal force (a), tangential force (b)

Definition of the stiffness K_n and k_s

The normal stiffness , K_n , and the tangential one, K_s , are functions of the distances between particles D_{eqSA} D_{eqNA} , of the surface S_a and also depend on the macroscopic parameter like the modulus of elasticity E and the Poisson ratio D (equation 8).

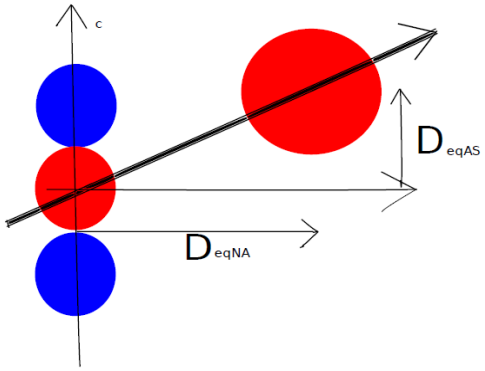

Figure 12: definition of the initial distance

$$\begin{cases} K_n = \dfrac{ES_a}{D_{eqNA}} \\ K_s = \dfrac{ES_a}{2(1+\nu)D_{eqSA}} \end{cases}$$

equation 8

$$S_a = \frac{4\pi R_a^2}{Nb_{ab}}$$

equation 9

Where S_a is the surface of the steel cylinder corresponding to the size of the steel element reduced by the number of concrete elements that link it, N_{bAB} (equation 9)

In graph 17 the interaction law is represented in function of the bar displacements.

Observation:

- With a normal displacement we have always an elastic phase , also beyond the value $S_a T_{NCmax}$ $S_a T_{NTmax}$.

- With a tangential displacement it is possible to identify three different phase :

$$\begin{cases} elastic\ phase: F \le F_e\ where\ F_e = S_a T_e \\ plasticity\ phase: F_e < F \le F_{max}\ where\ F_{max} = S_a T_{max} \\ friction\ phase: F > Fmax\ where\ F_{res} = S_a T_{res} \end{cases}$$

2.3.4 Mesh generation:

In the previous section are described the interaction laws between the particles. The specimen used for the simulation is designed with a huge number of spheres.
The first step is create a tetrahedral mesh ,inside the cylindrical specimen, with the program GMSH [http://geuz.org/gmsh] , [Geuzaine,2009] . The second step consists to filling with spheres the specimen starting from the mesh with tetrahedron previously obtained. The algorithm used is described in [Jevier, 2008]

2.3.5 Calibration of the parameters:

During the identification process the sample used must be isotropic in all the directions of contact . The radius of interaction is chosen to have an average of 12 interactions by particle [Rousseau, 2009]. With this interaction radius the values of α, β, γ determined by [Rousseau, 2009] are :

$$\begin{cases} \alpha = 3.7 \\ \beta = 2.198 \\ \gamma = 3.79 \end{cases}$$

The identification of the parameter can be split in two . First of all we have to calibrate the values of the Young's modulus and Poisson's ratio. When these values are determined we have to deal with the non-linear part of the stress/strain response. In the non linear part , the point is to identify local parameters to model macroscopic features such as compressive strength f_c and tensile strength f_t . The identification process starts with a tension test that gives us tensile local strength T and the softening parameters ζ . In a second phase the compressive test allows to check the softening parameters and to define C_o . Φi and Φc are fixed at 6° [Rousseau, 2009]. The frictional angle Φi must be between 5° and 15° to obtain a realistic behaviour. From [Camborde, 1982] we know that the contact angle Φc does not have a strong effect on the rupture behaviour and it could be equal toΦi.

All these parameters are calibrated after the study of loading velocity. A loading velocity that does not influence the result will be used .

a) experimental results

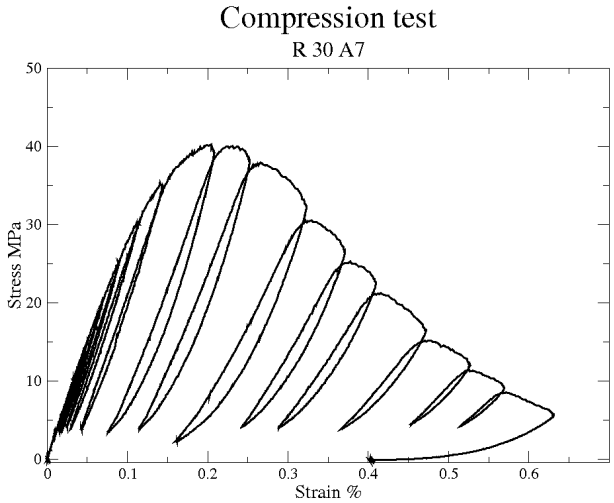

graph 18: experimental result L-3SR

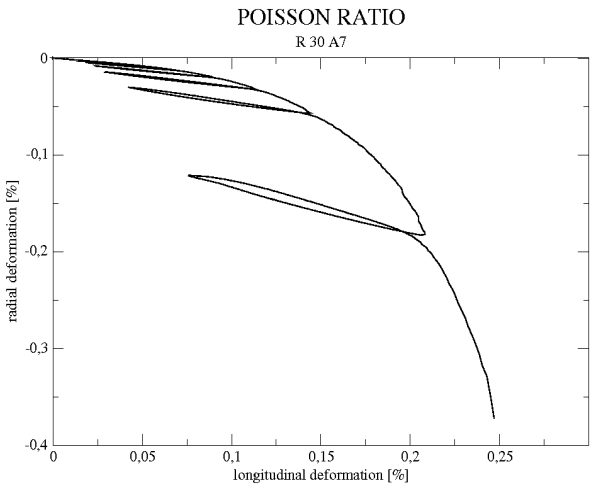

graph 19: experimental result L-3SR

We will present a calibration of the parameters for the concrete R30 A7. The main features for this concrete are in table 4 , they are calculated from the follow chart :

R30A7		
YOUNG' S MODULUS	E GPa:	31
POISSON RATIO	ν :	0.17
COMPRESSIVE STRENGTH	f_c MPa:	40
TENSILE STRENGTH:	f_t MPa:	4

Table 4

The values reported in (table 4) are obtained from the compression test done in L3R-S. f_t is taken as 10 % f_{tc} .

INFLUENCE OF THE VELOCITY

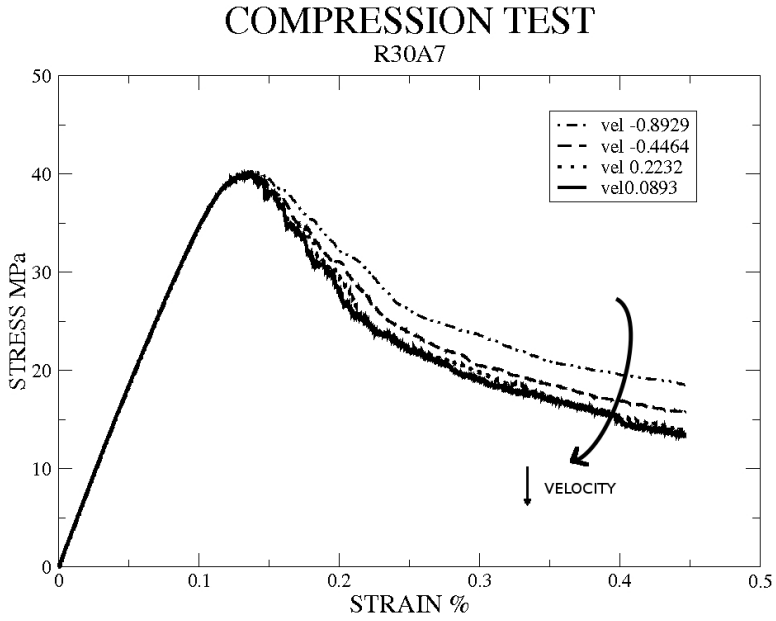

graph 20: compression test 30RA7

In graph 20 we want to show we are in a static case. The two smaller velocities in converge, therefore for our computations we chose the bigger of the last two (0.223 m/s).

Remark:

We also performed the calibration of the velocity for the traction test and we have obtain the convergence at the same loading velocity ratio.

Now we have to calibrate the discrete element parameter : the linear parameters , Young's Modulus & Poisson's ratio , and the non linear one.

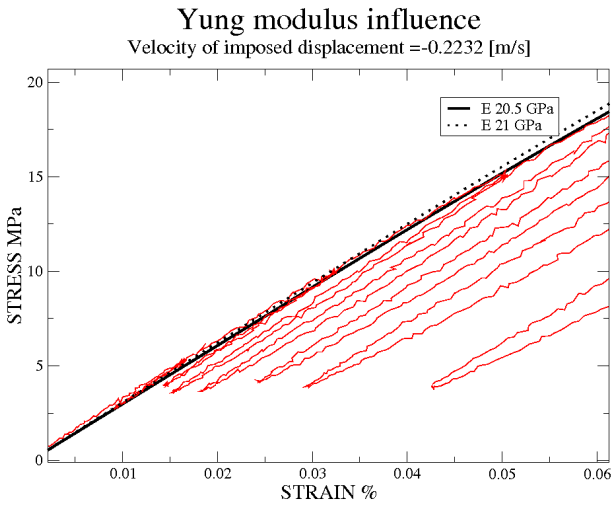

Graph 21 :Young's Modulus R30 A7

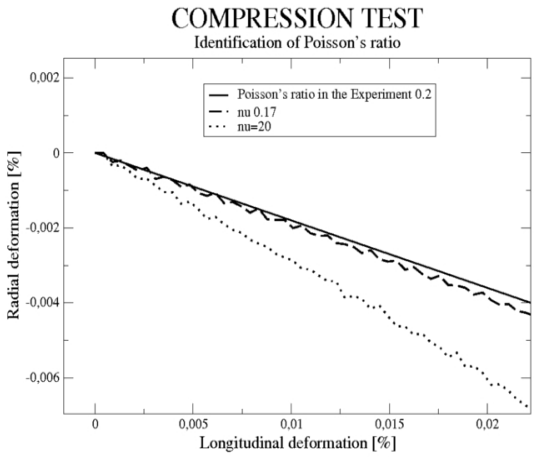

graph 22: Poisson's ratio R30 A7

The two straight line in graphs 21 & 22 represent the value in the linear part of the test. The good values to represent in the model the sample of concrete are E= 20.5Gpa and ν=0.13.

The calibration of the non linear parameters must to be done iteratively because we are dealing with three parameters that influence at the same time the compressive and the tensile behaviour. We can notice once again the effectiveness of discrete element modelling, in the fitting of the experimental result.

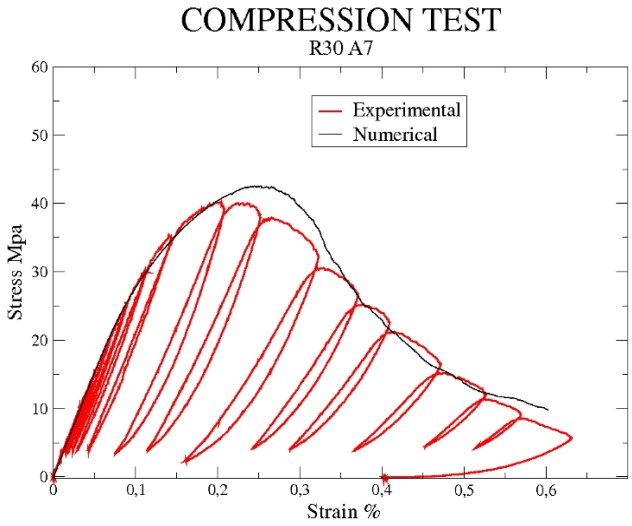

graph 23 : Experimental and Numerical results

3.Pull-out test

3.1 Introduction

We want to represent with the DEM the experimental results obtained in [Malvar, 1992] . To do so we run numerical simulations that consider a compression and traction test on a cylinder sample that has the same dimensions than the sample used in pull-out test. We generate six different meshes with the same dimension but differing for the mean radius of the sphere. The biggest mean radius of the spheres is equal to 3.1E-3 and the smallest one is equal to 1E-3 . As more widely described in the followings , we notice that the number of particles in the mesh changes a lot the value of the parameters needed to characterize the concrete. We expect a convergence decreasing the mean radius of the particles. When all the parameters are determined we look for the influence of radial pressure . We will base on pull-out test with radial pressure around the sample.

In (figure13) are represented a sketch of the sample used in the test and the specimen generated to do the computation.

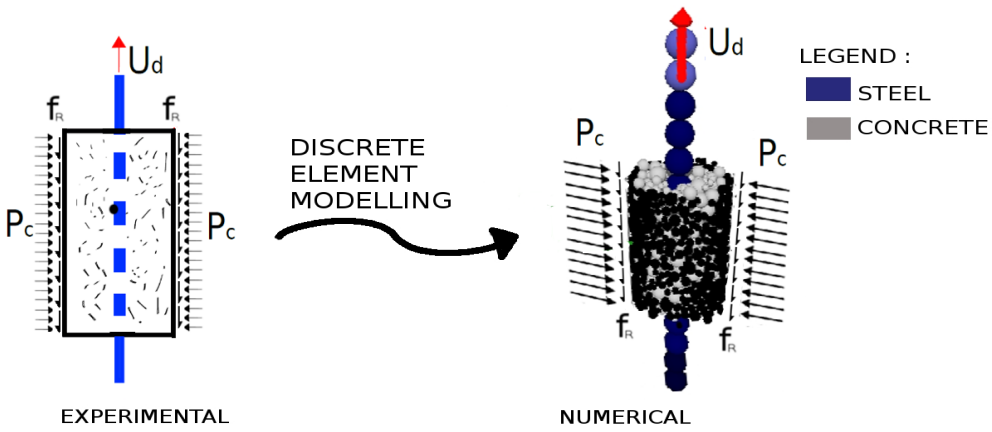

Figure 13 : Sketch of Experimental specimen [Malvar , 1992] and specimens used for numerical computation

Description of the specimen used for the DE computation :

With the code used, we are not able to apply a radial pressure . Only pressure in the axial directions can be simulated. We have built a software that exactly allows us to apply a radial pressure on the externals particles (black spheres in the figure 13) .For this particles the displacements along the bar axis are forbidden. The steel bar is represented by an aligned group of spheres having the same diameter than the bar. To hold the steel bar back, two particles at the bottom are blocked and in the meantime a displacement is imposed on the two spheres at top . From the imposed displacement we can compute the force so that we can evaluate the shear stress at the bar surface.

3.2 Concrete parameters calibration

3.2.1 Calibration for the first mesh:

The following calibration takes the mesh with mean radius equal to 0.0031 .

INFLUENCE OF VELOCITY:

Compression test:

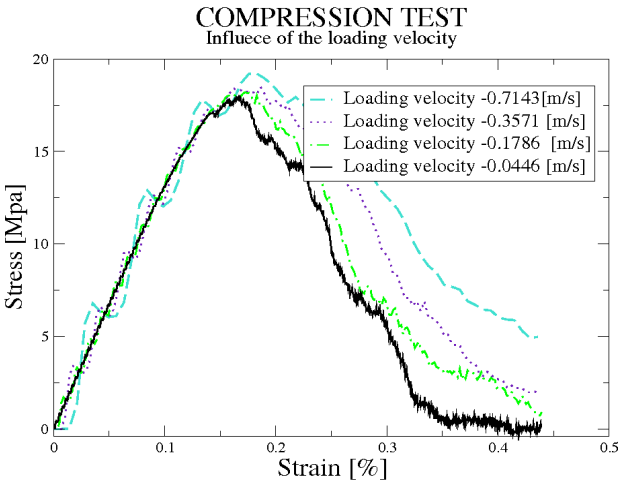

graph 24: Study of velocity, high values

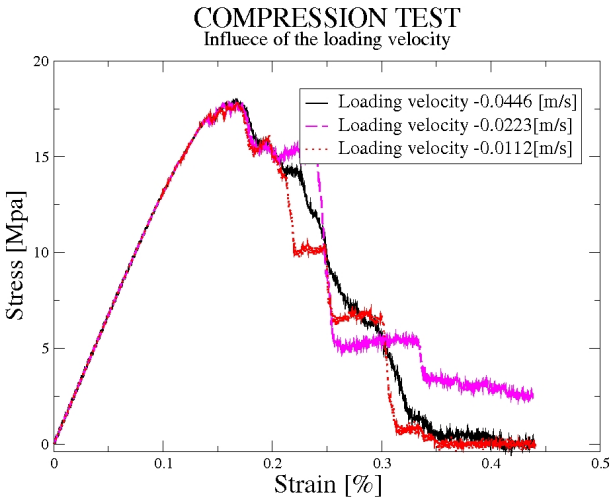

graph 25: Study of velocity,low value

Observation:

- In (graph 24), is shown the stress/strain relation with variations of the velocity from 0.7143 to 0.0446 m/s For the higher values of loading velocity many oscillation phenomena occur due to dynamic effect.
- In (graph 25),it is shown how a further decrease of the loading velocity leads to a steeped path in the post peak area . The presence of steps might be linked to a sudden decrease of stiffness probably due to the propagation of crack.
- We choose the velocity 0.0446 m/s because dynamic effect don't take place .In this assumption the static validity is checked.

Tension test :

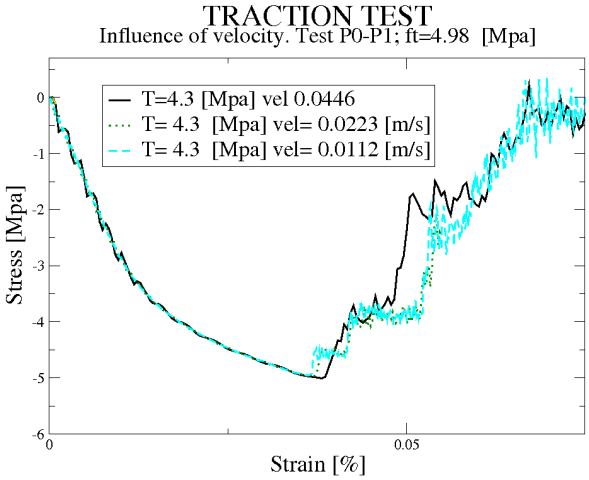

graph 26: velocity influence in traction test

The first attempt has been performed with the same velocity as in the compression test . We observe oscillation in the softening part of the curve. It is due to the fact that damping is not taking into account in this model.

The same velocity , 0.0446 m/s ,is chosen for traction and compression test .

LINEAR PARAMETERS: Young's modulus and Poisson's ratio

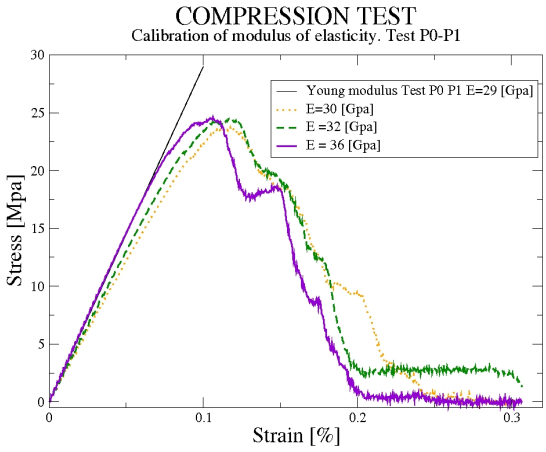

Graph 27 :Young' s modulus

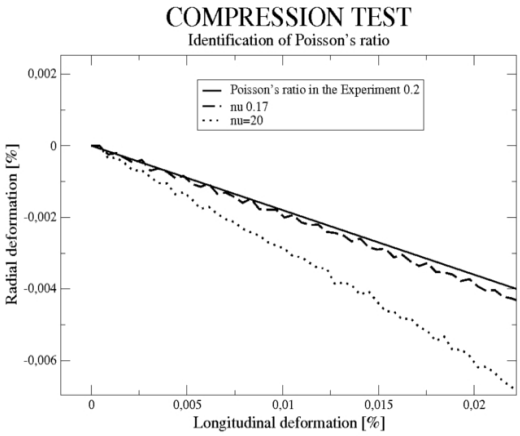

Graph 28 : Poisson's Ratio

The two straight line in the graph represent the value in the elastic part of elastic modulus and Poisson's ratio. The good values to represent in the model the sample of concrete are E= 36 Gpa and ν=0.17. It is worth noting that we have to take particular attention at the value of Poisson's ratio because the contraction or the expansion of the concrete is very important for the bond strength.

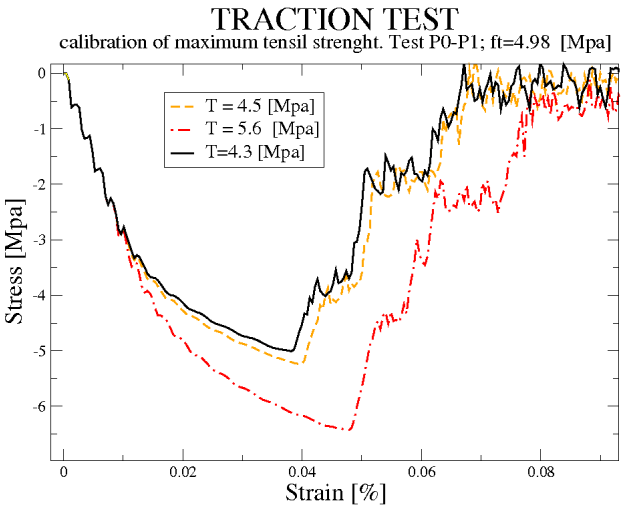

graph 29: T influence

TENSILE LIMIT:

An increase of T causes an increment of the strain and traction strength. It is also worth to note that the compressive strength increase with the growing of T .

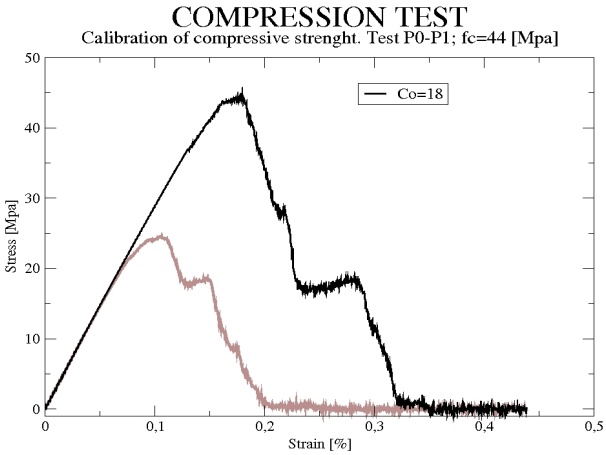

graph 30: Co influence

COMPRESSION LIMIT

When Co increase we have an increasing of the peak .

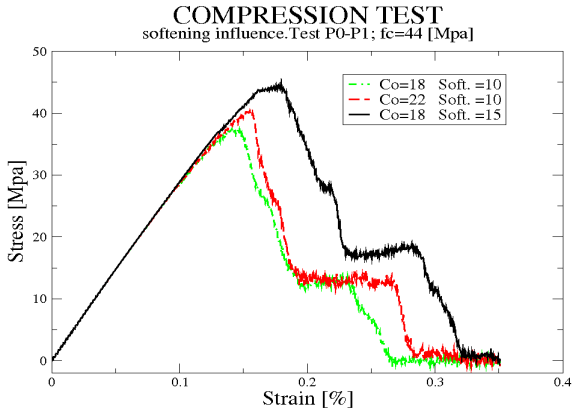

graph 31: Adou influence

SOFTENING

The softening is an influence parameter either for compression and traction. In particular here we note that the peak in compression increases of 15% when the increment of softening is 50%.

DAMPING

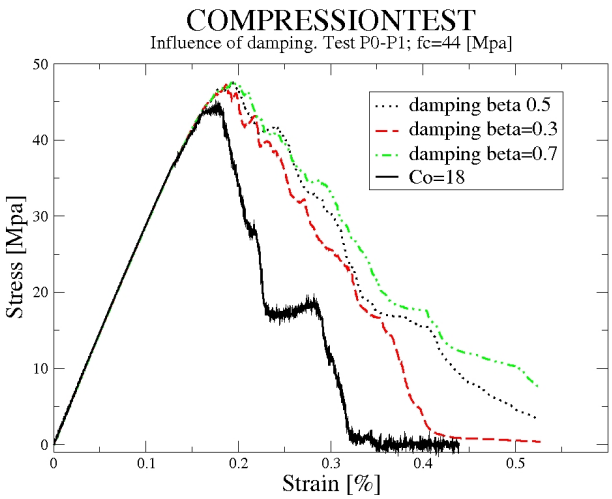

graph 32 :damping influence

The graph at the left represents the stress slip relationship in the concrete without the damping . In this curve we have oscillations, to delete it we can introduce a damping. An external force F_{amort} of the form:

$F_{amort} = -2\beta\omega M v$ where $\omega = 2\pi f$.

The curve green red and black represent the response of the system when we consider also the damping. The value of β differs in the three curve . Is interesting to remark that with the damping the external forces will be modified;

3.2.2 Influence of the mean radius on the parameter value :

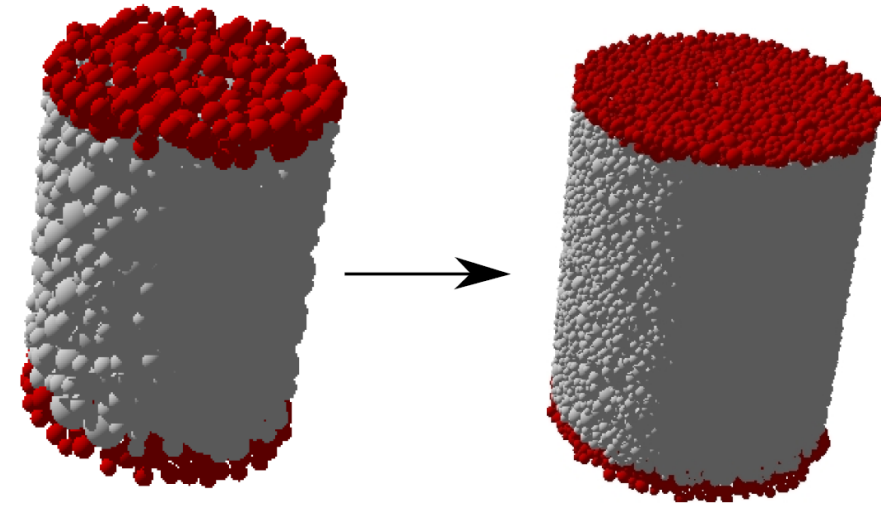

Figure 14: specimens representation

The follow table presents how the mean radius of the mesh particles influences the calibration of the parameter.

	MESH 1	MESH 2	MESH 3	MESH 4	MESH 5	MESH 6
Mean radius	0.0031	0.0029	0.0022	0.0014	0.0010	0.0007
Interaction radius	1.2356	1.3092	1.3689	1.3872	1.3940	1.401797
Elastic modulus GPa	36	25	20	20	18.3	18.3
Poisson's ratio	0.18	0.18	0.17	/	/	/
T parameter	4.3	3.5	2.7	/	/	/
Co parameter	18	11	8.1	/	/	/
Adou	15	10	10	/	/	/

Table 5

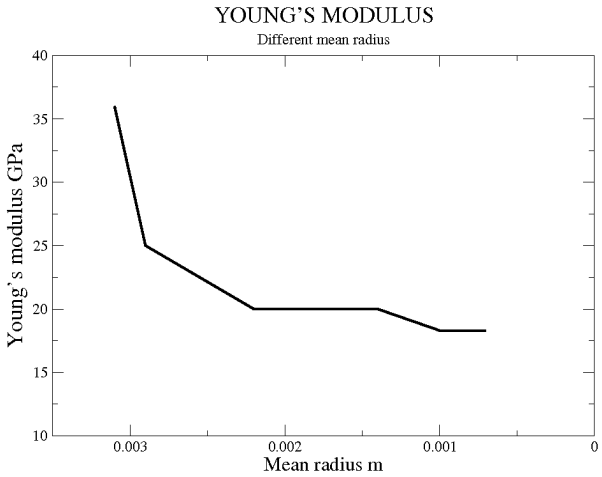

Graph 33: mesh influence

For the first three meshes shown in the (table 5) all the parameters are calibrated . It will be better to use a mean radius that doesn't influence the calibration value of the parameters but ,the computation time prevent this choice; for example simulating a compression test with the particles mean radius of 0.0007 , that's mean 132849 spheres, the time requite is roughly two months. The convergence is reached for a mean radius less than or equal to less than 1 mm.

3.3 Steel concrete interface parameters

3.3.1 Introduction

The interaction law at the microscopic level in the used code is in function of nine parameters, the influences of each parameters will be presented in the following. The aim of this section is to identify the values for the microscopic parameter in order to obtain with the numerical simulation the same stress/slip curve reported in [Malvar, 1992] .In Eurplexus code nine parameters are control the steel concrete interface (called BIMA) : E , nu , T_n , C_n ,

T_e , T_{max} , U_{max} , Φ_i, and Φ_c . To know how a single parameter influence the macroscopic behaviour that we set at the beginning all the data at high value and we change only one single parameter for each simulation . If all the parameters are set at very high values the link between concrete and steel doesn't reach the failure therefore the failure take place only between the concrete particles (that means that we simulate splitting, transverse & conic cracks).

3.3.2 Concrete law [Rousseau 2009]

Starting from the work [Rousseau 2009], we want to find the parameters of steel/concrete interface that allows us to fit the experimental curve [Malvar, 1992].

Identification of the parameters for pull out test without lateral confinement (testP0).

The parameter value used for the concrete [1] are reported in: table 5 column 2

Now is presented the calibration process related to Test P0 [Malvar 1992]. The results obtained are plotted in the following charts.

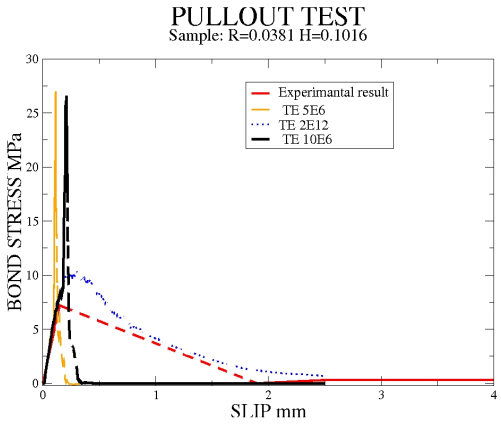

graph 34: TE

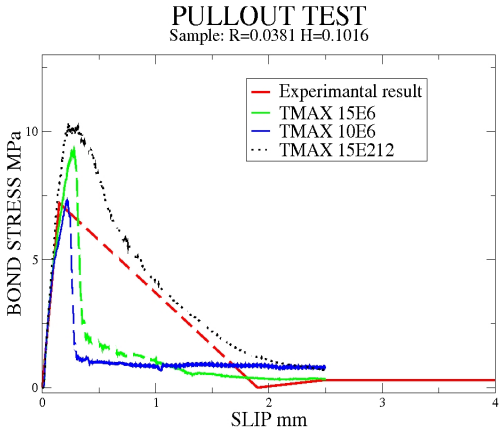

graph 35: Tmax

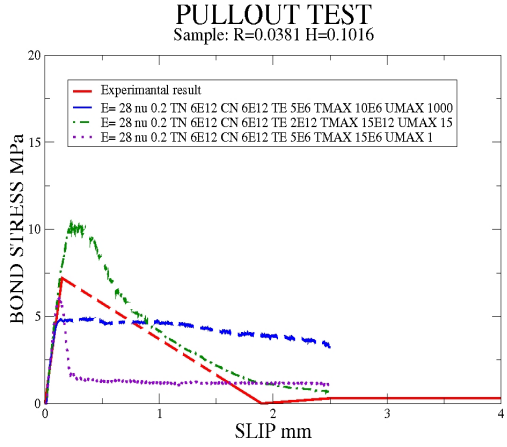

graph 36:Umax

In graphs 34-35-36 the parameters that govern the shear resistance of the steel/concrete link are shown. As shown by the chart graph 34 the parameter T_E has an influence on the elastic zone and on the value of maximum slip.

Graphs 35-36 show the influence of the maximum strength T_{max} and the maximum slip U_{max} .

The following graphs 37-38 show the influence of CN and TN:

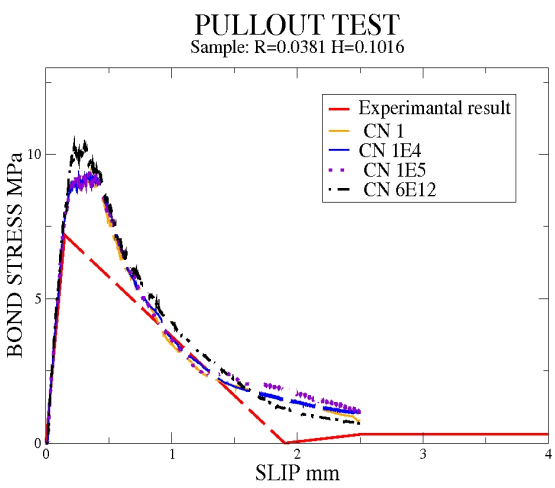

graph 37

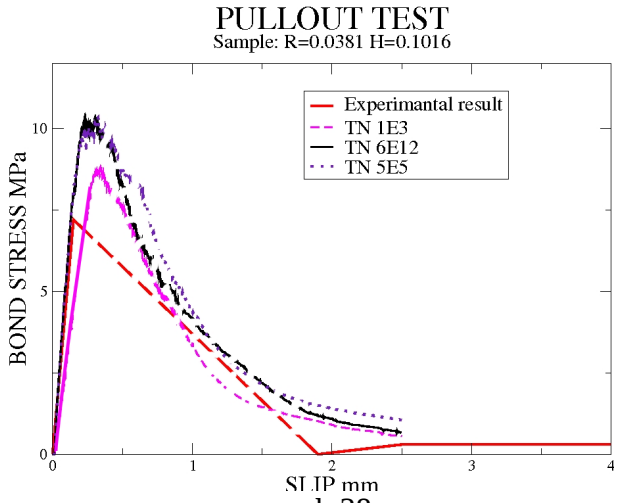

graph 38

TN and CN influences the normal maximum strength of the steel/concrete link (graph 17) . In graph 38 we note that with the decreasing of the value of TN, the first part of the slope decreases the inclination. Furthermore it is possible to note that the maximum bond stress reach lower values . CN affects mainly the maximum value of bond stress and trend near the peak.

Keeping in mind this observation we try to fit as well as possible the experimental result.(graph 39).

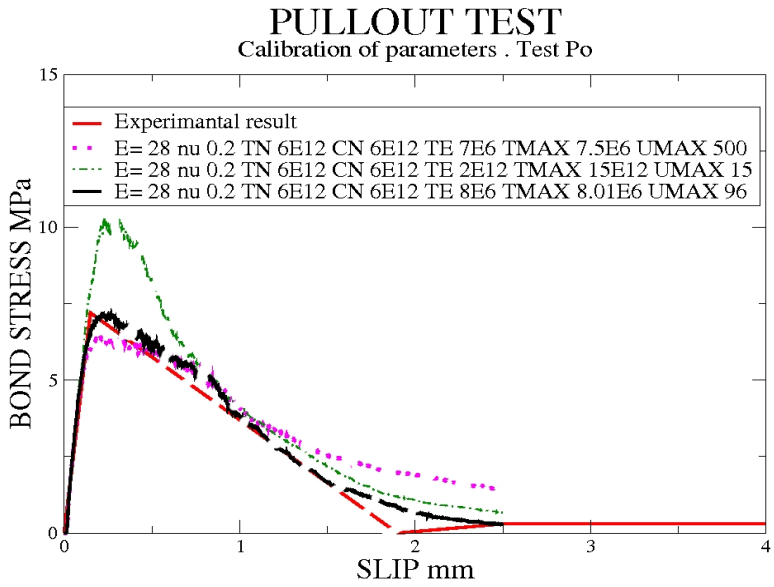

graph 39: Experimental and Numerical results.

The curve found with the computation fit very well the a numerical one. We want to determine which values must to be changed in the steel/concrete parameters in order to fit the experimental results when a radial pressure is applied .

Influence of the lateral pressure.

After the identification of the BIMA [P0] parameters a radial pressure is applied on the specimen during the pullout test .The starting value for the BIMA parameter are the values determined previously test P0 . Graph 40 show the experimental result compared with the numerical one ,it is clear that the numerical stress-slip curve are far from the experimental result.

It is also worth note that the pressure influences the stress-slip values until 10,24 MPa then any further variation of the pressure values does not influence any more the behaviour of the stress-slip curve.

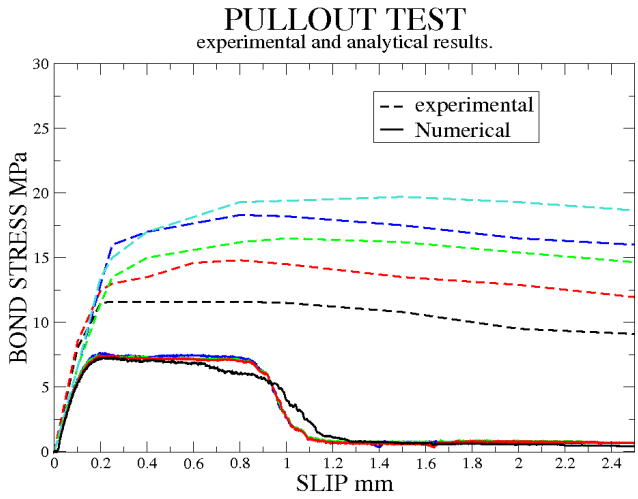

graph 40: BIMA[P0]. Zoom of the first slip part

We compute the stress/slip curves with high value for all the steel/concrete parameters. In this way the steel/concrete bond is always in the elastic domain and never reaches the failure . The results are shown in graph 41-42.

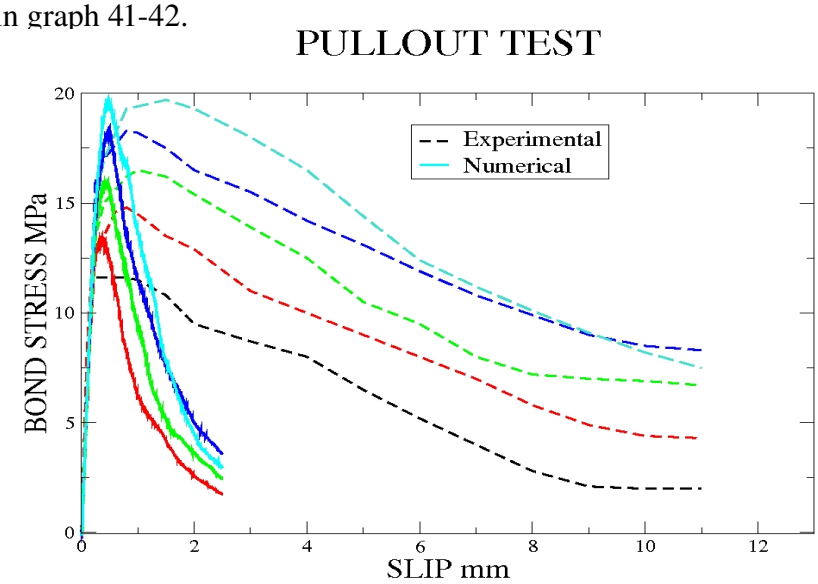

graph 41: concrete 1. BIMA with high value.

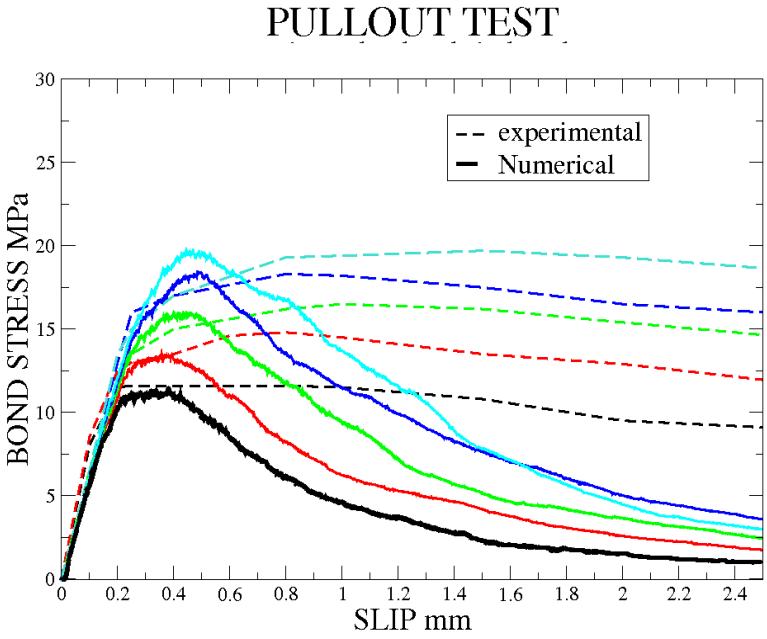

graph 42: concrete 1. BIMA with high value.
Zoom of the first slip part

We observe that the numerical curves reaches the peak values, with a good approximation, but in the post- peak the curves are still far from a good convergence. Therefore in this case with steel/concrete parameters we can't reproduce the experiment.

New parameter for the concrete

The idea now is to change the non linear parameters for concrete (Table6) .

MESH 2 (table 3)	CONCRETE [1]	CONCRETE [2]	CONCRETE [3]
Elastic modulus GPa	25.04.00	25,4	25,4
Poisson's ratio	0.18	0.18	0.18
T parameter	3.5	2.1	2,2
Co parameter	11	9	6
Softening	10	30	30

Table 6

Once again the numerical stress/slip curve fit the experimental results when no radial pressure is applied.

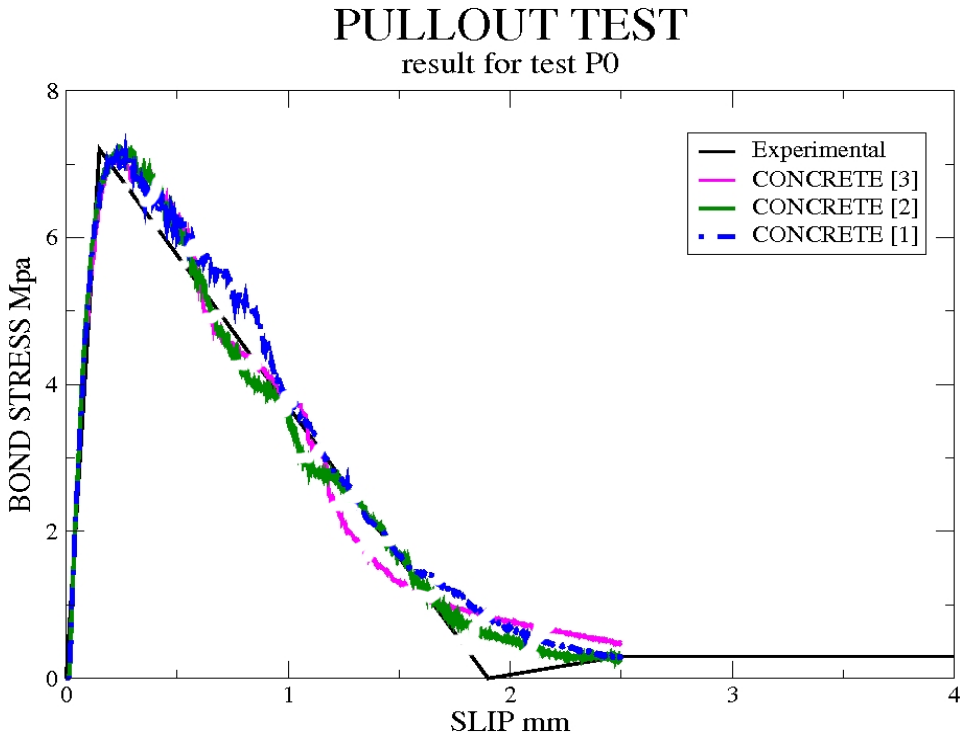

graph 43 : experimental and numerical curve .

The value used to calibrate the steel/concrete interface changes in function of the concrete considered (table 7):

Mesh [2]			
BIMA PARAMETERS	CONCRETE [1]	CONCRETE [2]	CONCRETE [3]
E	28	28	28
nu	0,2	0,2	0,2
T_n	6,00E+012	1,00E+006	1,00E+006
C_n	1,00E+012	1,00E+012	1,00E+012
T_e	8,00E+006	8,00E+006	8,00E+006
T_{max}	8,01E+006	8,50E+006	8,50E+006
U_{max}	96	150	110
Φ_i,	15	15	15
Φ_c	15	15	15

Table7

We have run the first computation with very high values for the BIMA parameters (graph 44-45)

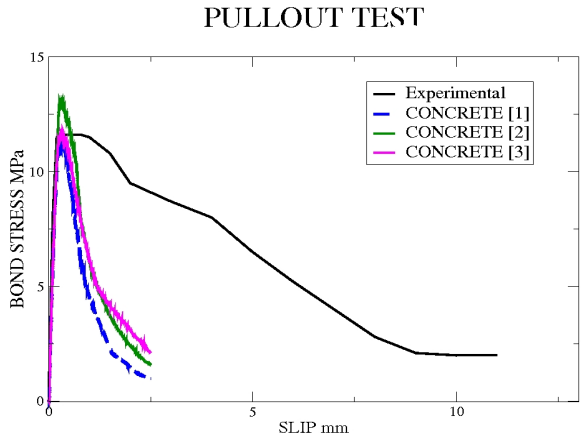

graph 44: Test 1 numerical and experimental curve

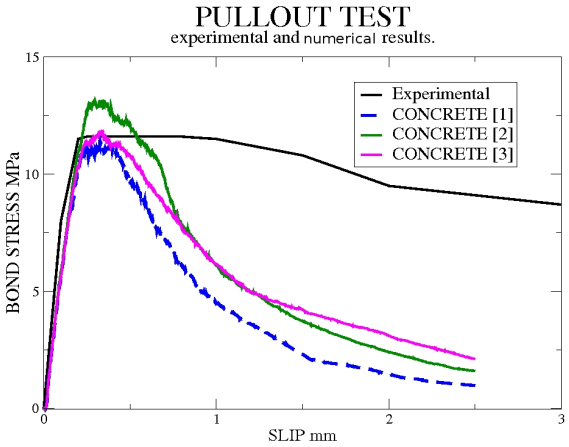

graph 45: Test 1 numerical and experimental curve. Zoom of the first part

The convergence is not reached in this case. BIMA parameters have not influential here because if we decrease their values some other broken links between discrete element particles appear and, therefore, the numerical stress/slip curve goes further than the experimental one.

3.3.3 New concrete law [Marin, 2009]

Introduction

Now we change the concrete law in the EUROPLEXUS code . The new concrete law used takes into account the effect of confinement [Marin, 2009] . The main characteristics of the compaction law are explained in the followings.

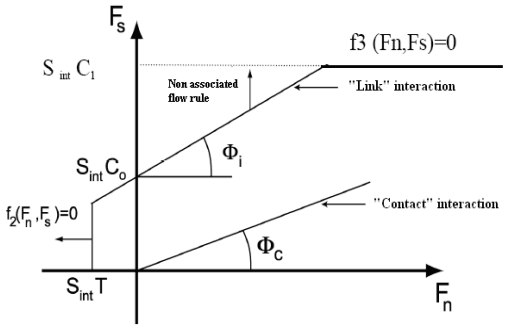

Graph 46 : Interaction law

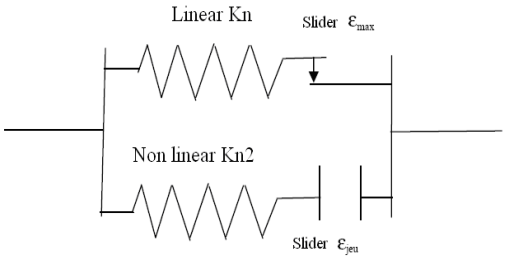

Figure 15 : link between concrete spheres

Normal stiffness: the linear elastic spring is coupled in series with a slider . This set is coupled in parallel with a non-linear spring of stiffness K_{n2} that is activated starting from a normal strain value threshold ε_{jeu}.

Tangential stiffness: To increase this value we changed the sliding criterion by limiting the increase of the maximum possible shear force .

Computation :

In graph 47 the difference between the two different concrete laws are shown:

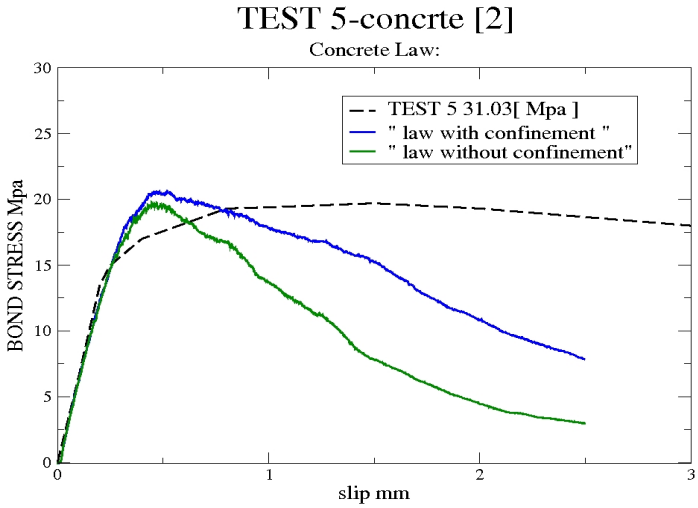

graph 47: influence of the concrete law

The curve with the compacting law of concrete decrease its slope in the post peak part.

We are looking for a good fitting between the numerical and experimental bond/slip curve when the higher lateral pressure is applied.

Calibration of the softening:

We remark that little variation of softening changes a lot the behavior of the curve.

Softening “ADOU70” & “ADOU200”:

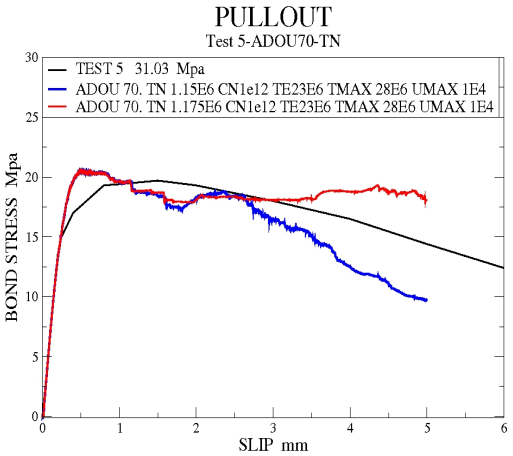

graph 48: ADOU67.TN sensibility

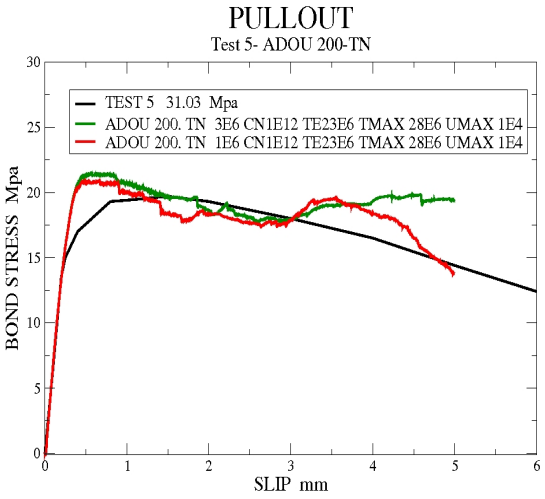

graph 49: ADOU200 .TN sensibility

In (graph 48 - 49) is shown the sensitivity to the TN value, due to this sudden variations of the curves after little variations of TN, any further calibration is impossible in the studied case.

3.3.4 New steel/concrete interface law

Another possible approach consist to modify the current law of steel/concrete interface , presented in the section 2.3.3c . The main characteristics of the current steel/concrete law are:

Fn=f(Un) : the normal force depends by the normal displacements

Fs=f(Us) : the tangential force depends by the tangential displacements.

The proposed change is :

Fn=f(Un) : the normal force will depends by the normal displacements

Fs=f(Us;Fn) : the tangential force will depends by the tangential displacements and by **the normal force** (graph 50)

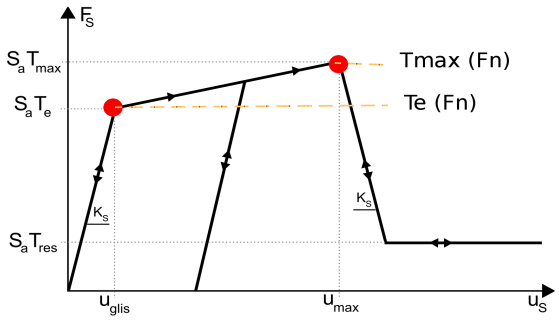

graph 50: modification proposed for the steel/concrete law

3.3.5 Further improvement of the current concrete/interface interaction law

In this research the experimental test results found by Malvar in 1992 have been used to develop the improvement of the steel concrete interaction law for the DEM. As mentioned in the section 2.2.5 the pull out test with lateral pressure done by Malvar consists of two series :

- test 1- 5: Bars with inclined ribs that have a 68-deg angle with longitudinal axis are used.
- test 6- 10: Bars with inclined ribs that have a 90-deg angle with longitudinal axis are used.

In [Malvar,1992] is demonstrated that the geometry of the lugs influences the bond resistance in a lateral confinement pull-out test . Is worth to note that in the current law there is no parameter that permits to consider the lugs shape influences (section 3.3). Two possible working methods which will allow us to consider the influence of the lugs are suggested below:

1. Change the number of particles (figure 16 c), used to describe the steel bar; represent the lugs with a series of particles with the diameter equal to the width of the lugs. This way could be proper but the time required for the calculus will be prohibitived for the simulation.
2. Represent the surface of the bar as a rigid boundary surrounded by an assembly of a big numbers of spheres modelling the concrete. A similar approach, with reference to a more simple interface geometry, was used in [Calvetti, 2001] to simulate the interaction of a pipeline with the surrounding soil.

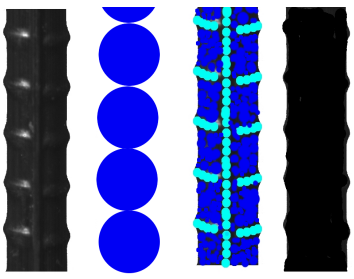

Figure 16: (a) real bar. (b) current method (c) hyp 1 (D) hyp 2

4. Conclusions

The pullout test reported in [Malvar, 1992] has been chosen to calibrate the parameters of the Discrete Element Method to represent reinforced concrete.

The DE steel/concrete law [Rousseau, 2009] allow to simulate the pullout test without confinement (graph 39); therefore, from the test with no lateral pressure applied we deduce the steel/concrete parameter values .With the determined parameter values we have computed the pullout simulation with lateral pressure in order to see if there is influence on the stress/slip curve (graph 40). The set of parameters used until now of the steel/concrete does not allows us to obtain the experimental curve (graph 42).

Since we do not have the whole compression and traction stress/strain curve for the concrete used in [Malvar ,1992] but only the compression strength f_c and the traction one f_t (table 2) we have tried different combinations of the non-linear parameters for the concrete to fit them. Three different kind of concrete is used in the numerical test but the stress/slip curve once again is far from the experiment (graph 44-45) .

We have modify the current law in the model with the concrete compaction law [Marin, 2008] To take into account the confinement pressure also for the concrete behaviour .An appreciable fitting is obtain (graph 47) but not enough to reach a good result.

We remark in the last simulation that the dangerous sensitivity to the BIMA value TN , representing the limit in traction for steel/concrete sphere, (graphs 48-49) do not permit to do any good calibration. Additional studies should be done to understand the instability in the bond/slip curve generated by the material parameters of DEM in order to fit the experimental behavior.

REFERENCES :

[Calvetti 2001] F.Calvetti , C. Di Prisco, R. Nova “Modelling of pipeline landslide interaction” 2001

[Camborde 1999] F.Camborde “ modelization du comportement dynamique de béton-application aux problemes d'impact et d'explosions “, thése d'Ecole Central de Nantes 1999

[Clément , 1987] J-L Clément, “Interface acier-béton et comportement des structures en béton armé - caractérisation – modélisation” Thése de doctorat de l'université de Paris 6, 1987.

[C. K. Soh 1999] C. K. Soh, S. P. Chiew, Y. X. Dong, Damage model for concrete-steel interface, Journal of Engineering Mechanics p979-982,

[Cowell 1982] Cowell, A. D., Bertero, V. V. and Popov “an investigation of local bond Dorr slip under variation of speciment parameters” 1982

[Cundall ,1979] Cundall and Strank “ A Discrete numerical model for granular assemblies,1979

[Daud 2003] Daud “Etude expérimentale de la liason entre l'acier et le béton autoplacant contribution à la modelisation numérique de l 'interface. Thèse de l'INSA de Toulouse.

[Dominguez 2005] N. Dominguez Ramirez, “Etude de la liaison Acier-Béton : De la modelisation du phénomène à la formulation d'un élément enrichi <<béton armé>> “, PhD thesis LMT Cachan, 2005

[Dorr 1978] Dorr, K., “bond behaviour of ribbed Reinforcement Under transverse pressure” 1978

[Eligehasen 1982] Rolf Eligehasen, Egor P. Popov, Vitelmo V. Bertero , “ Local bond stress-slip relationships of deformed bars under generalized exitations” Report to the National Science Foundation ,University of California ,Berkeley 1982

[Geuzaine,2009] C. Geuzaine and J.-F. Remacle. “Gmsh: a three-dimensional finite element mesh generator with built-in pre- and post-processing facilities.International Journal for Numerical Methods in Engineering” Volume 79, Issue 11, pages 1309-1331, 2009

[Goto 1971] Cracks formed in concrete around tension bars.ACI Journal; Vol.38

(4) pp. 244-251.

[Gambarova ,1982] Gambarova P.G. And Karakoç, C "Shear -confinement interaction at the bar to concrete interaface" 1982

[Gambarova ,1983] Gambarova P.G. And Chiamulera, G.B. "Test results concerning the confinement effects on steel to concrete bond , after concrete splitting along the reinforcing bar" 1983

[Gambarova, 1989] Gambarova P.G. , Rosati G.P. , Zasso B. "Steel-to-concrete bond after concrete splitting: test results" 1989

[Gambarova ,1996] Gambarova P. G , Rosati G.P. , "Bond and splitting in reiforced concrete : test result on bar pull-out" 1996

[Gambarova , 1997] Gambarova P.G. , Rosati G.P., Schumm C.E. " Bond and splitting: a vexing question" 1997

[Hentz, 2003] Hentz V. Donzé,Daudeville, "Discrete element modelling of concrete submitted to dynamic loading at high strain rates" 2003

[Jerier, 2008] Jerier,Imbault,Donze,Doremus " A geometric algorithm based on tetrahedal meshes to generate a dense polydisperse sphere packing"2008

[Malvar, 1992] L. Javier Malvar " Bond of Reinforcement Under Controlled Confinement " 1992

[Marin, 2008] P.Marin, L.Daudville,J.Rousseau,E. Frangin "caracterisation et modelisation du comportement macanique des betons sous tres fort confinement" Grenoble 2008

[Nachtsheim 82] W. Nachtsheim & F. Stangenberg. "Interpretation of results of meppen slab tests – comparison with parametric investigations." Nuclear Engineering and Design, vol. 75, pages 283–290, 1982.

[Prado ,2003] E.P. Prado, J.G.M. Van Mier " Effect of particle structure on mode I fracture process in concrete" 2003

[Rousseau 2009] Jessica Rousseau, Philippe Marin, Laurent Daudeville, Sergueï Potapov, "Coupling Discrete Elements with Shell Finite Elements to simulate impacts on reinforced concrete structures"

[Untrauer 1965] Untrauer, R. e. and Henry , R.L., "Inflence of normal pressure on bond strength" ACI journal,proceedings, Vol 62, No 5, May

1965

[V.Donze 2003] V.Donze “ Spherical Discrete Elements Code” 2003

[Viwathanetepa1979] Viwathanetepa,S., Popov, E.P., and Bertero, V.V., “Effects of Generalized Loading on Bond of Reiforcing Bars Embedded in Confined Concrete Blocks” 1979

[V.Mier 97] J.G.M. Van Mier. “Numerical analysis of interface fracture in concrete using in lattice type fracture model.” Int. J. of damage Mechanics, vol. 6, pages 408–432, 1997.